NASA TECHNICAL NOTE

NASA TN D-2326

NASA TN D-2326

AN EXPERIMENTAL INVESTIGATION OF HIGHLY UNDEREXPANDED FREE JETS IMPINGING UPON A PARALLEL FLAT SURFACE

by Allen R. Vick and Earl H. Andrews, Jr.

Langley Research Center
Langley Station, Hampton, Va.

NATIONAL AERONAUTICS AND SPACE ADMINISTRATION • WASHINGTON, D. C. • JUNE 1964

AN EXPERIMENTAL INVESTIGATION OF HIGHLY UNDEREXPANDED FREE JETS IMPINGING UPON A PARALLEL FLAT SURFACE

By Allen R. Vick and Earl H. Andrews, Jr.

Langley Research Center
Langley Station, Hampton, Va.

NATIONAL AERONAUTICS AND SPACE ADMINISTRATION

For sale by the Office of Technical Services, Department of Commerce,
Washington, D. C. 20230 -- Price $1.50

AN EXPERIMENTAL INVESTIGATION OF HIGHLY UNDEREXPANDED FREE JETS IMPINGING UPON A PARALLEL FLAT SURFACE

By Allen R. Vick and Earl H. Andrews, Jr.
Langley Research Center

SUMMARY

An investigation to determine the effects of highly underexpanded free jets impinging upon an adjacent flat surface has been conducted. The experimental program conducted in the Langley 41-foot vacuum sphere consisted of obtaining pressure measurements and high-speed schlieren photographs. Unheated air (of approximately 2,400 lb/sq in. abs) was exhausted from two different nozzles, a converging nozzle (jet exit Mach number, 1.0; nozzle exit diameter, 0.125 inch) and a converging-diverging nozzle with a nominal design Mach number of 5.0 having a nozzle exit diameter of 0.625 inch. The jet-impingement surface was mounted parallel to the nozzle axial center line and the distance of this surface from the nozzle axis was varied for each of the test nozzles. Continuous data were obtained over a range of ratios of jet total pressure to ambient pressure varying from about 250,000 down to 20,000.

The data are reported herein together with certain correlations of the pressure distributions along a line parallel to the nozzle axial center line. The location of the peak static-pressure ratio appeared to correspond to the location of the oblique shock which is formed downstream of the initial impingement point. For the two closest plate positions, the jet-impingement-point variation is relatively small over the range of total-pressure ratios investigated and results in a relatively constant location of the peak surface-static-pressure ratios. At large distances of the jet-impingement surface from the nozzle, a change in the type of flow experienced on the surface occurs which results in more than one peak static-pressure ratio. For relatively close plate locations and for a given location on the plate, it was further observed that the ratio of surface pressure to total pressure remained essentially constant as the ratio of total pressure to ambient pressure was varied. Angles between the flow direction at the initial jet-impingement point and the plate surface ranging from 58° to 65° and 33° to 41° for the Mach number 1.0 and Mach number 5.0 nozzles, respectively, corresponded to critical values for which the peak surface pressure shifted from a position a considerable distance downstream of the initial jet-impingement point up to the vicinity of jet impingement.

INTRODUCTION

Rocket exhaust gases expanding into the vacuum of outer space leave the nozzle in a highly underexpanded condition. Under such circumstances these exhaust gases on leaving the nozzle exit flow in a radial direction which, at the jet plume boundary, may be nearly perpendicular to the nozzle thrust axis. Typical problems arising as a result of these large billowing jet plumes include high-altitude stage separation (ref. 1), attitude control for space rendezvous missions, soft lunar landings and take-off (refs. 2, 3, and 4), and structural and heating problems brought about by direct impingement of the hot exhaust gases on adjacent vehicle surfaces. The purpose of this experimental investigation was to determine the pressure distributions associated with highly underexpanded free jets impinging upon adjacent flat surfaces. A similar investigation with a somewhat different objective using a Mach number 2.0 nozzle, tests being conducted over a range of ratios of jet total pressure to ambient pressure up to about 14,000, is presented in reference 5. Another investigation (ref. 6) presents experimental data for a 2:1 area ratio nozzle at pressure ratios $\left(p_{t,j}/p_\infty\right)$ up to about 2,350. Included was a comparison of experimental results with theoretically predicted surface pressure distributions using a method based on Newtonian flow theory.

The investigation reported herein was conducted in the Langley 41-foot vacuum sphere, data being obtained in the form of surface pressure measurements and high-speed schlieren photographs. Cold-air tests, with a total temperature of about 90° F, were conducted at stagnation pressures of approximately 2,400 lb/sq in. abs with two different nozzles, a converging nozzle (jet exit Mach number, 1.0) and a converging-diverging nozzle (jet exit Mach number, 5.0). The jet-impingement surface was a flat plate mounted parallel to the nozzle axial center line and the distance of this surface from the nozzle axial center line was varied for each of the test nozzles. The range of ratios of jet total pressure to ambient pressure was from about 250,000 down to 20,000.

SYMBOLS

d_j	nozzle exit diameter
M_j	nozzle exit Mach number
p_j	nozzle exit static pressure
p_s	static pressure on impingement surface
$p_{t,j}$	nozzle total pressure
p_∞	vacuum sphere ambient pressure
x	distance along impingement surface measured axially from nozzle exit
y	distance between impingement surface and center line of nozzle
R	radial distances from center of impingement surface (see fig. 2)
ψ	angle in degrees measured clockwise with respect to nozzle axial center line (see fig. 2)

θ_n half-angle of nozzle

β angle between tangent to jet boundary and impingement surface at point of impingement

α_n angle between tangent to jet boundary and jet axis immediately after expansion to ambient pressure at nozzle exit

$\Delta\left(\frac{x}{d_j}\right)$ distance between point of impingement and location of maximum surface pressure

ν_n Prandtl-Meyer expansion angle corresponding to nozzle exit Mach number

ν_1 Prandtl-Meyer expansion angle corresponding to jet boundary Mach number

APPARATUS AND PROCEDURE

Test Setup and Procedure

The experimental investigation was conducted in the Langley 41-foot vacuum sphere with the test setup as shown in figure 1(a). Air from a tank farm pressurized to approximately 2,400 lb/sq in. abs was supplied to the nozzles, located near the center of the sphere, through a 3/4-inch-diameter supply pipe. The volume of air available was sufficient to maintain essentially a constant nozzle stagnation pressure during a test run. An enlargement of the test setup, shown in the schematic in figure 1(b), shows the general arrangement of the nozzle, impingement surface, and schlieren mirror. The impingement surface, a flat plate with dimensions of 36 inches by 42 inches, was mounted parallel to the nozzle axial center line. Surface pressure distributions were measured with the plate located at distances corresponding to 7, 14, 30, and 60 nozzle exit diameters away from the $M_j = 1.0$ nozzle center line and 2, 4, 6, and 10 nozzle exit diameters from the $M_j = 5.0$ nozzle center line. The location of the plate center point downstream of the nozzle exit varied with the distance between the plate and the nozzle center line in order to obtain a better coverage of surface pressures in the vicinity of the jet-impingement point.

Vacuum pumps were utilized to attain initial pretest pressures in the sphere of approximately 0.4 mm Hg (0.0077 lb/sq in. abs). An electrically operated solenoid valve located just upstream of the nozzle permitted a rapid start. For one sphere evacuation, two 15-second runs were made with a brief shutdown between the two runs for the purpose of reloading the motion-picture camera. During the total test time of approximately 30 seconds, the pressure ratio was reduced from about 250,000 down to about 20,000. With the test nozzle in operation the sphere pressure increased linearly with time; therefore, the ratio of total pressure to ambient pressure decreased hyperbolically with time.

Some of the symbols and parameters used in the discussion are defined by the sketch in figure 1(c).

Test Nozzles

Tests were conducted with two nozzles, one convergent and the other convergent-divergent, as shown in figure 1(d). The converging nozzle $\left(M_j = 1.0\right)$ had an exit diameter of 0.125 inch and the converging-diverging conical nozzle of nominal design Mach number of 5.0, based on inviscid flow, had an exit diameter of 0.625 inch, an expansion area ratio of 25, and a half-angle of 15°. For some tests conducted with the nominal $M = 5.0$ nozzle, a static-pressure orifice installed in the expansion wall just upstream of the exit indicated an actual exit Mach number of 4.79.

The initial turning angle of the flow at the nozzle exit α_n, obtained from measurements of a series of schlieren photographic enlargements at known values of the ratio of nozzle total pressure to ambient pressure, indicated a substantially larger value of the effective expansion half-angle θ_n at the exit than the inviscid design value. This comparison was performed by using an expression, $\alpha_n = \nu_1 - \nu_n + \theta_n$ (see, for example, ref. 7). With ν_n and ν_1 determined from the estimated exit Mach number of 4.79 and the experimental value of the ratio of ambient pressure to total pressure, respectively, the effective nozzle half-angle was computed to be 26.5° or about 11.5° greater than the inviscid design value. Reference 8, in which small-scale high Mach number nozzles were tested, experienced a similar phenomenon in that measured values of α_n were considerably different from the calculated values. A comparison of the difference between measured and calculated values of α_n, when correlated with the Reynolds number of about 13×10^6 based on nozzle exit conditions and diffuser conical length, indicates favorable agreement with the same type of correlation as shown in reference 8. For large-scale configurations, it is believed that θ_n should correspond to the geometric angle; however, more research is needed in this area.

Instrumentation

Nozzle stagnation pressure was measured by a 3,000 lb/sq in. abs pressure transducer located between the electrically operated solenoid valve and the nozzle inlet bell. The sphere ambient pressure was measured in the vicinity of the nozzle by a small differential pressure transducer with a range of 0.005 to 0.10 lb/sq in. abs. The impingement plate was instrumented with static orifices 0.040 inch in diameter located as shown in figure 2. All static orifices were connected to differential pressure transducers (NACA miniature-type inductive gage) by means of 9-inch lengths of tubing to reduce possible vibrational effects and yet retain a rapid response system. All pressure measurements were continuously recorded on oscillographs for the duration of each 15-second test.

High-speed double-pass schlieren movies (16 millimeter) were obtained for each test run. A 25-inch-diameter parabolic mirror was mounted about 4 feet behind the nozzle (as shown in fig. 1(a)) and the viewing port and camera were located on the equator of the vacuum sphere in the monitoring room. By properly synchronizing the motion-picture camera with the flashing schlieren light source, maximum frame rates of about 750 frames per second were obtained. Timing marks recorded on the edge of the motion-picture film from a 60-cycle flashing light source permitted a correlation of pressure ratio with time for each test run.

RESULTS AND DISCUSSION

Tabulated Data

The investigation reported herein contains results obtained with two different nozzles $\left(M_j = 1.0 \text{ and } M_j = 5.0\right)$ having exhaust plumes impinging upon a parallel adjacent flat surface. The tabulated data of this investigation are presented in table I for the $M_j = 1.0$ nozzle for values of plate distances away from the nozzle of 7, 14, 30, and 60 nozzle exit diameters and in table II for the $M_j = 5.0$ nozzle at plate distances of 2, 4, 6, and 10 nozzle exit diameters. Columns (1) to (5) of the tables contain data in a nondimensional ratio form of surface static pressure to ambient pressure p_s/p_∞ for five constant values of ratios of nozzle total pressure to ambient pressure $p_{t,j}/p_\infty$ ranging from 250,000 down to 50,000. Columns (6) to (10) contain the identical data converted to ratios of surface static pressure to nozzle total pressure $p_s/p_{t,j}$. In the polar coordinate sketch of figure 2 the nozzle axial center line is considered to be at $\psi = 0^\circ$ and data are tabulated at intervals of $22\frac{1}{2}^\circ$ as ψ increases in a clockwise direction. Data in the figures are primarily limited to those obtained on a line parallel to the nozzle axial center line $(\psi = 0^\circ)$; however, typical plots are presented showing how the data contained in the tables for pressure orifices other than along $\psi = 0^\circ$ might be used.

Experimental Results

General flow description.- A general inspection of the data indicates that the impingement of a supersonic jet on an adjacent surface produces surface pressure distributions strongly dependent upon the type of shock system produced by the impinging jet. There appears to be two different shock configurations experienced in this investigation which depended upon y/d_j, $p_{t,j}/p_\infty$, and nozzle geometry. It can be postulated that one such system occurred when the flow was turned at the point of impingement by an oblique shock system, and that the other occurred when the flow had too large an impingement angle to be turned by an oblique shock and, therefore, had to pass through a normal shock. However, for the latter case an oblique shock was formed downstream of the initial impingement point when the flow was able to negotiate the required turning angle.

Jet boundaries.- Theoretical jet plume boundaries calculated by the method of characteristics for quiescent air, using three-dimensional irrotational equations of flow, are shown in figure 3 for each of the ratios of nozzle total pressure to ambient pressure shown on the data sheets. The jet boundaries are presented in a nondimensional ratio form as the variation of y/d_j with x/d_j. Experimental boundaries obtained from photographic enlargements of individual frames from the schlieren movies (see figs. 4 and 5) are indicated by symbols. Excellent agreement with theoretical results is indicated over the complete range of pressure ratios for both nozzles. It should be emphasized here that the theoretical calculations, for the nominal $M_j = 5.0$ nozzle, were based on the actual exit Mach number of 4.79 and effective nozzle half-angle of $\theta_n = 26.5^\circ$ which are both considerably different from the inviscid design value. Superimposition on the jet-boundary plots of the various plate locations for the different test configurations permits a determination of the jet-impingement-point location.

At the extreme pressure ratios covered in this investigation (up to $p_{t,j}/p_\infty = 250{,}000$), the possibility of air condensation exists in that static temperatures occur below that required for condensation; however, because of the small model size and the time required for condensation to occur, the effects were believed to be negligible. Several factors appear to substantiate this belief. In view of the fact that viscous effects produced by formation of water droplets would retard the expanding gas velocity and affect the size of the jet plume, the excellent agreement of experimental and theoretical jet boundaries indicates that if condensation were present, its effects are minor. In addition, the rapid expansion of the free jet downstream of the nozzle exit results in a decreasing frequency of molecular collisions required for droplets to form and retards even further the possibility of condensation.

The oblique shock waves produced by jet impingement and obtained from high-speed schlieren movies are shown in figure 3(a) for the $M_j = 1.0$ nozzle at the two closest plate positions, $y/d_j = 7$ and 14, and in figure 3(b) for the nominal Mach 5.0 nozzle at $y/d_j = 2$. For these plate positions, no movement of the oblique shock could be detected as the pressure ratio decreased from 250,000 down to 50,000. As the impingement surface is moved out to a distance of 14 nozzle exit diameters, the oblique shock associated with the sonic nozzle impingement has about doubled in its location downstream of the nozzle exit, increasing from about 4 to 8 nozzle diameters. Further increases in distance between the nozzle and impingement surface result in a change in surface flow and a movement of the oblique shock up to the point of jet-boundary impingement.

Schlieren photographs.- Schlieren photographs obtained from the 16-millimeter motion-picture film are presented in figures 4 and 5 for the $M_j = 1.0$ and $M_j = 5.0$ nozzles, respectively. Enlargements of individual frames corresponding to the pressure ratios for which data are presented, with the exception of photographs for the $M_j = 1.0$ nozzle at $y/d_j = 30$ which were omitted because of their poor quality, are shown in chronological order in each figure. Theoretical jet plume boundaries are shown only once for each of the five different pressure ratios. (See figs. 4(b), 4(c), and 5(d).)

The initial jet-impingement point, partially obscured in some of the photographs, may be approximated from the shape of the free jet boundary on the opposite side of the nozzle. In general, the oblique shock that originates downstream of the initial impingement point is believed to be typical of the type III flow discussed in reference 5 in which significant flow separation occurs at the impingement point followed by an oblique shock with considerable flow separation along the surface. From the photographs it is further evident, however, that this thickly separated region persists only for a limited distance downstream of the initial impingement point (see fig. 4(a)) and then becomes very thin. As the pressure ratio is decreased, a second oblique shock forms far downstream of the nozzle exit and moves upstream. (See fig. 4(a).)

At the outermost plate location for the $M_j = 1.0$ nozzle (fig. 4(c)) the oblique shock appears to originate very close to the impingement point at the highest pressure ratios. The schlieren motion pictures show that as the pressure ratio decreases, the oblique shock changes into a series of short shocks, possibly of the type that would occur if vortices were present in the flow along the surface.

Schlieren photographs for the $M_j = 5.0$ nozzle at the closest plate location (fig. 5(a)) are basically similar to those for the $M_j = 1.0$ nozzle with the oblique shock originating several nozzle exit diameters downstream of the impingement point. As indicated in figure 5(a), however, the length of thick boundary layer on the impingement surface extends much further downstream than at comparable pressure ratios with the $M_j = 1.0$ nozzle. Increasing the distance between the impingement surface and the nozzle axis (figs. 5(b) and 5(c)) introduces a flow phenomenon considerably different from that noted in the foregoing discussion. These figures show two apparent shock systems (see fig. 5(b)) which have a tendency to coalesce as the pressure ratio decreases. The first shock originates at the impingement point and reduces in strength, as indicated by the decrease in angle between the shock and surface, as the pressure ratio decreases. The second shock adheres more closely to the surface than the initial shock and appears to originate somewhat downstream of the boundary impingement point. Adjacent to the surface and bounded by the second shock is a region containing apparently large-scale turbulence. Observations of this region in the motion-picture film showed that the turbulence consisted of a series of vortices which grew in size as the flow proceeded downstream.

Surface pressure distributions.- Examples of local variations of surface static-pressure ratio p_s/p_∞ with nozzle total-to-ambient pressure ratios for a few individual static-pressure orifices are shown in figure 6 for the $M_j = 1.0$ nozzle at spacing ratios of $y/d_j = 7$ and 60. This figure is typical of the type of curves from which the data presented in the tables were obtained. Figure 6(a) shows an essentially linear variation of surface pressure with the ratio of nozzle total pressure to ambient pressure which is typical for the pressure variation at all orifice locations for $y/d_j = 7$ and 14 for the $M_j = 1.0$ nozzle and $y/d_j = 2$ for the $M_j = 5.0$ nozzle. Nonlinear variations shown in figure 6(b) are typical of the outermost plate locations and show that as the pressure ratio is decreased, the impingement point moves downstream and crosses first one orifice location and then another and, as a result, there are local regions of high pressure.

Pressure distributions produced by impingement of the exhaust plume on a flat surface are shown in figures 7 and 8 for the $M_j = 1.0$ and $M_j = 5.0$ nozzle, respectively, as the variation of surface static-pressure ratio p_s/p_∞ with distance along the nozzle axial center line in terms of nozzle exit diameter ratio x/d_j. Maximum values of p_s/p_∞ of about 500 and 130 were obtained for the $M_j = 1.0$ nozzle $\left(y/d_j = 7\right)$ and $M_j = 5.0$ nozzle $\left(y/d_j = 2\right)$, respectively, at $p_{t,j}/p_\infty = 250{,}000$. In general, the data correspond to one of two flow configurations depending on y/d_j, $p_{t,j}/p_\infty$, and nozzle geometry. One flow configuration which appears to be independent of $p_{t,j}/p_\infty$ is characterized by an oblique shock located near the plate at an appreciable distance downstream of the jet-boundary-impingement point. Surface pressure ratio trends associated with this type of flow have peak values closely corresponding to the points of shock location as shown by comparing figures 7(a), 7(b), 7(c), and figure 8(a) with figures 3(a) and 3(b), respectively. This correlation occurs, regardless of the nozzle total-pressure ratio, at a relatively constant location downstream of the nozzle exit. The constant location of peak pressure is primarily a result of the fact that the jet-impingement-point variation is relatively small over the range of pressure ratios investigated as was shown in figure 3.

As the surface-to-nozzle separation distance is further increased, a limit is reached in which a change occurs in the surface flow characteristics. First evidence of this flow change is observed at $y/d_j = 30$ and $p_{t,j}/p_\infty = 50{,}000$ for the $M_j = 1.0$ nozzle, and $y/d_j = 4$ for the $M_j = 5.0$ nozzle at the lower pressure ratios. This second type of flow configuration is characterized by an oblique shock located at the jet-boundary-impingement point in which the peak surface pressure also occurs either at or very near the point of impingement. A comparison of figures 7(c) and 7(d) with figure 3(a) and figures 8(b), 8(c), and 8(d) with figure 3(b) shows this change in surface flow phenomena. These results are somewhat similar to those of reference 5 which showed peak surface pressures being produced at the impingement point for low pressure ratios with an apparent tendency toward a downstream movement of peak pressure at the higher pressure ratios.

The shift in peak pressure location with decreasing pressure ratio is a gradual occurrence as shown in figure 8(b). The initial peak pressure decreases in prominence with decreasing pressure ratio and also moves downstream at a rate closely approximated by the shift in jet-impingement-point location. Concurrent with the decrease in initial peak pressure is a gradual increase in prominence of the pressure at the point of jet impingement. These trends indicate a decrease in shock strength at the downstream location and an increase in shock strength at the impingement point.

The distributions of the surface static pressures expressed as a ratio to the nozzle total pressure $p_s/p_{t,j}$ are presented in figures 9 and 10. At the closest plate position $\left(y/d_j = 7;\ \text{fig. } 9(a)\right)$, a single curve is drawn to represent the average variation of $p_s/p_{t,j}$ for the complete range of test pressure ratios. That a single curve can be drawn for a range of pressure ratios indicates that the surface pressure at a given location relative to the nozzle exit is directly proportional to the nozzle total pressure and is independent of the ratio of nozzle total pressure to ambient pressure. Figures 9(b) and 10(a) indicate a slight increase in the span of maximum and minimum surface pressures brought about by the increased range of the jet-impingement-point location.

Figures 9(c), 10(b), and 10(c) show that higher absolute values of peak surface pressure may exist at the lower pressure ratios (see, for example, curves for $p_{t,j}/p_\infty = 250{,}000$ and 50,000), depending on whether the oblique shock is located at the point of jet-boundary impingement or downstream of this location. This condition may be the result of lower total pressure losses being incurred at the lower pressure ratio for which the angle of jet impingement is least.

Radial and circumferential distributions.- The previous discussion has been restricted solely to the surface pressure distributions along a line parallel with the nozzle axial center line. Typical variations of $p_s/p_{t,j}$ with R/d_j are presented in figure 11(a) for the plate position $y/d_j = 7$, and a pressure ratio $p_{t,j}/p_\infty = 250{,}000$ along radial lines identified in the insert sketch. Circumferential plots of the surface pressure distribution at various radii are shown in figure 11(b). By plotting both radial and circumferential pressure distributions and cross checking between the two curves, it was possible to improve the fairing of each individual curve, particularly those with a limited number of data points. All points used to construct a given curve that were arrived at through interpolation are shown as crossed (×) symbols. Deviations from symmetrical patterns of pressures are relatively small as can be seen in the circumferential plots in figure 11(b). Typical plots for the $M_j = 5.0$ nozzle constructed similar to those for the $M_j = 1.0$ data are shown in figures 12(a) and 12(b).

Jet-impingement angle.- Results of a correlation of the angle β between the jet boundary and impingement surface with the shift in peak pressure location are shown in figures 13(a) and 13(b) for the $M_j = 1.0$ and $M_j = 5.0$ nozzle, respectively. The impingement angle β, as obtained from both schlieren and theoretical results, is plotted against $\Delta\left(\frac{x}{d_j}\right)$ which is the distance between the jet-boundary-impingement point, as obtained from figures 3(a) and 3(b), and the peak pressure location as obtained from the pressure-distribution plots. Curves of constant pressure ratio and plate location are shown for each of the test nozzles, dashed lines indicating extrapolation in the region of shifting peak pressure location. The critical angles of jet impingement for which the peak pressure shifts in location occur in the range from about 58° to 65° for the Mach 1.0 nozzle and from 33° to 41° for the Mach 5 nozzle. This range of about 7° appears to remain relatively constant for both nozzles over the range of pressure ratios investigated. As $p_{t,j}/p_\infty$ increases, the impingement angle for which maximum surface pressure will exist at the point of initial jet-boundary impingement also increases.

A comparison of figures 13(a) and 13(b), at constant plate locations from the nozzle axis, indicates that peak pressures occur much farther downstream of the initial jet-impingement point $\Delta\left(\frac{x}{d_j}\right)$ for the $M_j = 1.0$ nozzle than for the $M_j = 5.0$ nozzle. At pressure ratios extrapolated to values greater than those of this investigation, but at the same plate locations y/d_j, little change in location of peak pressure is indicated for the $M_j = 5.0$ nozzle, whereas significant increases may be expected for the $M_j = 1.0$ nozzle. These data indicate that in order to achieve a relatively constant location of maximum surface pressure over a large range of pressure ratios, it is necessary to use either a high Mach number nozzle or else maintain a small separation distance between the nozzle and impingement surface.

SUMMARY OF RESULTS

An investigation to determine the effects of highly underexpanded free jets impinging upon an adjacent flat surface has been conducted. The experimental program conducted in the Langley 41-foot-diameter vacuum sphere consisted of obtaining pressure measurements and high-speed schlieren photographs. Unheated air (of approximately 2,400 lb/sq in. abs) was exhausted from two different nozzles, a converging nozzle (nozzle Mach number of 1.0 and nozzle diameter of 0.125 inch) and a converging-diverging nozzle (nominal design Mach number of 5.0 having a nozzle diameter of 0.625 inch). In general, the data corresponded to one of two flow configurations on the impingement surface depending on the distance separating the plate from the nozzle center line, the value of the ratio of nozzle total pressure to ambient pressure, and the nozzle design. The following results were obtained:

1. The locations of the free-jet boundary-impingement points on the adjacent parallel flat plate were determined experimentally and theoretically and correlated with the locations of the peak pressure ratios measured on the flat plate.

2. One flow configuration was characterized by an oblique shock located an appreciable distance downstream of the jet-boundary-impingement point. The maximum pressures measured on the plate were obtained at the oblique shock location for the smallest plate spacing; a maximum pressure 500 times ambient pressure was measured for the Mach 1.0 nozzle and 132 times ambient for the nominal Mach 5.0 nozzle. Near linear variations of the ratios of surface static pressure to ambient pressure with ratios of jet total pressure to ambient pressure were obtained for the Mach 1.0 nozzle at all orifice locations for the two closest plate locations. For relatively close plate locations, the pressures measured at any position on the plate were very close to being directly proportional to the nozzle flow total pressure and were independent of ambient pressure.

3. The second flow configuration was characterized by an oblique shock located at the point of jet-boundary impingement on the plate. For the Mach 1.0 nozzle, this flow configuration was first obtained when the plate position or

jet pressure ratio was altered in such a way that the jet-boundary-impingement angle was reduced to some value within the range from 58° to 65° depending on the particular value of pressure ratio. For the nominal Mach 5.0 nozzle, the corresponding range of impingement angles extended from about 33° to 41°. Maximum surface pressures were much lower with this particular type of flow than when the oblique shock was located some distance downstream of the jet-boundary-impingement point.

4. These data indicate that in order to achieve a relatively constant location of maximum surface pressure over a range of pressure ratios, it is necessary to use either a high Mach number nozzle or else maintain a small separation distance between the nozzle and impingement surface.

Langley Research Center,
National Aeronautics and Space Administration,
Langley Station, Hampton, Va., February 18, 1964.

REFERENCES

1. Peters, Tom, Christenson, R. J., and Dawson, J. G., Jr.: Impingement Effects of a Model SLV-5 Second-Stage Jet Plume on the First-Stage Booster Cases at Altitudes From 65,000 to 91,000 Ft. AEDC-TDR-63-7. Arnold Eng. Dev. Center, Mar. 1963.

2. Stitt, Leonard E., and Latto, William T., Jr.: Highly Underexpanded Exhaust Jets Against Adjacent Surfaces. Astronautics and Aerospace Eng., vol. 1, no. 1, Feb. 1963, pp. 107-110.

3. Eastman, Donald W., and Radtke, Leonard P.: Flow Field of an Exhaust Plume Impinging on a Simulated Lunar Surface. AIAA Jour. (Tech. Notes and Comments), vol. 1, no. 6, June 1963, pp. 1430-1431.

4. Roberts, Leonard: The Action of a Hypersonic Jet on a Dust Layer. Paper No. 63-50, Inst. Aerospace Sci., Jan. 1963.

5. Bauer, R. C., and Schlumpf, R. L.: Experimental Investigation of Free Jet Impingement on a Flat Plate. AEDC-TN-60-223 (Contract No. AF 40(600)-800 S/A 11(60-110)). Arnold Eng. Dev. Center, Mar. 1961.

6. Margolin, E. L., and Welch, Eugene: Final Report - Single Nozzle Jet Plume Test in the Rocket Nozzle Test Facility. SID 63-426, North American Aviation, Inc., May 6, 1963.

7. Latvala, E. K.: Spreading of Rocket Exhaust Jets at High Altitudes. AEDC-TR59-11, ASTIA Doc. No. AD-215866 (Contract No. AF 40(600)-700 S/A 13(59-1)), Arnold Eng. Dev. Center, June 1959.

8. Falanga, Ralph A., Hinson, William F., and Crawford, Davis H.: Exploratory Tests of the Effects of Jet Plumes on the Flow Over Cone-Cylinder-Flare Bodies. NASA TN D-1000, 1962.

TABLE I.- SURFACE PRESSURE DATA RESULTS OF $M_j = 1.0$ NOZZLE EXHAUST PLUME IMPINGING UPON AN AXIALLY PARALLEL ADJACENT PLATE

(a) $\frac{y}{d_j} = \frac{0.875}{0.125} = 7$

Orifice	$\frac{x}{d_j}$	$\frac{R}{d_j}$	ψ, deg	① p_s/p_∞ for values of $p_{t,j}/p_\infty$ of -	②	③	④	⑤	⑥ $p_s/p_{t,j}$ for values of $p_{t,j}/p_\infty$ of -	⑦	⑧	⑨	⑩
				250,000	200,000	150,000	100,000	50,000	250,000	200,000	150,000	100,000	50,000
1	-8	16	180	1.38	1.00	0.63	0.26	0.18	0.0055×10^{-3}	0.0050×10^{-3}	0.0042×10^{-3}	0.0026×10^{-3}	0.0036×10^{-3}
2	-4	12		4.60	3.19	2.02	.90	-----	.0184	.0160	.0135	.0090	------
3	0	8		77.80	61.00	45.00	29.30	14.00	.3112	.3050	.3000	.2930	.2800
4	4	4	↓	495.00	397.00	298.20	199.50	99.00	1.9800	1.9850	1.9880	1.9950	1.9800
5	8	0	180, 0	446.00	356.30	266.50	175.30	86.00	1.7840	1.7815	1.7767	1.7530	1.7200
6	12	4	0	251.20	200.50	150.00	99.50	48.70	1.0048	1.0025	1.0000	.9950	.9740
7	16	8		138.00	110.00	82.50	54.20	26.70	.5520	.5500	.5500	.5420	.5240
8	24	16		35.85	28.40	21.15	13.95	6.80	.1434	.1420	.1410	.1395	.1360
9	32	24		14.50	10.60	6.90	3.55	1.00	.0580	.0530	.0460	.0355	.0200
10	40	32		8.10	5.60	3.80	2.20	.75	.0324	.0280	.0253	.0220	.0150
11	56	48		3.28	2.44	1.72	1.12	.50	.0131	.0122	.0115	.0112	.0100
12	72	64		1.74	1.31	.90	.51	.40	.0070	.0066	.0060	.0051	.0080
13	104	96		.84	.50	.49	.72	.63	.0034	.0025	.0033	.0072	.0126
14	136	128		.89	.82	.74	.82	.74	.0036	.0041	.0049	.0082	.0148
15	168	160	↓	1.08	.77	.67	.53	-----	.0043	.0039	.0045	.0053	------
5		0	22.5	446.00	356.30	266.50	175.30	86.00	1.7840	1.7815	1.7767	1.7530	1.7200
28		72	↓	1.18	1.00	.74	.41	.46	.0047	.0050	.0049	.0041	.0092
27		136		.76	.72	.67	.69	.51	.0030	.0036	.0045	.0069	.0102
16		16	225	4.10	2.95	2.06	1.23	.24	.0164	.0148	.0137	.0123	.0048
5		0	225, 45	446.00	356.30	266.50	175.30	86.00	1.7840	1.7815	1.7767	1.7530	1.7200
21		16	45	31.90	24.90	17.90	11.10	5.00	.1276	.1245	.1193	.1110	.1000
22		48		2.13	1.65	.90	------	------	.0085	.0083	.0060	------	------
23		84		.77	.62	.51	.67	.50	.0031	.0031	.0034	.0067	.0100
24		112		.85	.65	.68	.58	.33	.0034	.0033	.0045	.0058	.0066
25		144		.65	.72	.60	.66	.60	.0026	.0036	.0040	.0066	.0120
26		176	↓	.90	.57	.24	------	-----	.0036	.0029	.0016	------	------
5		0	67.5	446.00	356.30	266.50	175.30	86.00	1.7840	1.7815	1.7766	1.7530	1.7200
29		72	67.5	.65	.55	.44	.56	-----	.0026	.0028	.0029	.0056	------
18		8	270	120.00	95.80	71.50	47.50	22.80	.4800	.4790	.4767	.4750	.4560
5		0	270, 90	446.00	356.30	266.50	175.30	86.00	1.7840	1.7815	1.7768	1.7530	1.7200
19		8	90	120.00	95.70	71.50	47.40	23.00	.4800	.4785	.4767	.4740	.4600
30		32	90	1.67	1.40	.94	.46	.14	.0067	.0070	.0063	.0046	.0028
20		16	315	34.10	26.80	19.50	12.30	5.65	.1364	.1340	.1300	.1230	.1130
5		0	315, 135	446.00	356.30	266.50	175.30	86.00	1.7840	1.7815	1.7768	1.7530	1.7200
17		16	135	3.59	2.65	1.97	1.16	.32	.0144	.0133	.0131	.0116	.0064

TABLE I.- SURFACE PRESSURE DATA RESULTS OF $M_j = 1.0$ NOZZLE EXHAUST PLUME IMPINGING UPON AN AXIALLY PARALLEL ADJACENT PLATE - Continued

(b) $\frac{y}{d_j} = \frac{1.750}{0.125} = 14$

				1	2	3	4	5	6	7	8	9	10
Orifice	$\frac{x}{d_j}$	$\frac{R}{d_j}$	ψ, deg	p_s/p_∞ for values of $p_{t,j}/p_\infty$ of -					$p_s/p_{t,j}$ for values of $p_{t,j}/p_\infty$ of -				
				250,000	200,000	150,000	100,000	50,000	250,000	200,000	150,000	100,000	50,000
1	-8	16	180	1.67	1.37	0.62	0.13	0.23	0.0067×10^{-3}	0.0069×10^{-3}	0.0041×10^{-3}	0.0013×10^{-3}	0.0046×10^{-3}
2	-4	12	↓	5.34	4.58	3.45	.33	-----	.0214	.0229	.0230	.0033	------
3	0	8		27.70	21.30	14.90	8.70	9.70	.1108	.1065	.0993	.0870	.1940
4	4	4		91.00	73.00	55.00	36.20	17.30	.3640	.3650	.3667	.3620	.3460
5	8	0	180, 0	139.80	111.60	83.20	54.60	26.10	.5592	.5580	.5547	.5460	.5220
6	12	4	0	148.40	118.40	88.50	58.50	28.20	.5936	.5920	.5900	.5850	.5640
7	16	8		116.60	93.30	69.60	45.70	22.20	.4664	.4665	.4640	.4570	.4440
8	24	16		55.20	43.90	32.70	21.60	10.50	.2208	.2195	.2180	.2160	.2100
9	32	24		24.50	18.40	12.50	7.20	2.70	.0980	.0920	.0833	.0720	.0540
10	40	32		13.24	10.09	7.06	4.23	1.68	.0530	.0505	.0471	.0423	.0336
11	56	48		5.15	3.91	2.93	1.85	.88	.0206	.0196	.0195	.0185	.0176
12	72	64		2.54	1.98	1.37	.77	.23	.0102	.0099	.0091	.0077	.0046
13	104	96		.88	.71	.52	.60	.55	.0035	.0036	.0035	.0060	.0110
14	136	128		.57	.58	.74	.76	.70	.0023	.0029	.0049	.0076	.0140
15	168	160	↓	.82	.69	.80	.46	-----	.0033	.0035	.0053	.0046	------
5		0	22.5	139.80	111.60	83.20	54.60	26.10	.5592	.5580	.5547	.5460	.5220
28		72	↓	1.77	1.47	1.00	.55	.20	.0071	.0074	.0067	.0055	.0040
27		136		.79	.75	.89	.62	.47	.0032	.0038	.0059	.0062	.0094
16		16	225	4.52	3.85	4.23	1.85	-----	.0181	.0193	.0282	.0185	------
5		0	225, 45	139.80	111.60	83.20	54.60	26.10	.5592	.5580	.5547	.5460	.5220
21		16	45	49.00	38.60	28.10	17.90	8.30	.1960	.1930	.1873	.1790	.1660
22		48		3.88	2.74	1.36	------	-----	.0155	.0137	.0091	------	------
23		84		1.02	.80	.56	.43	.38	.0041	.0040	.0037	.0043	.0075
24		112		.54	.59	.61	.42	.23	.0022	.0030	.0041	.0042	.0046
25		144		.80	.76	.75	.63	.66	.0032	.0038	.0050	.0063	.0132
26		176	↓	.68	.48	.14	-----	-----	.0027	.0024	.0009	------	------
5		0	67.5	139.80	111.60	83.20	54.60	26.10	.5592	.5580	.5547	.5460	.5220
29		72	67.5	1.08	.81	.49	.23	-----	.0043	.0041	.0033	.0023	------
18		8	270	76.00	60.10	44.20	28.80	13.50	.3040	.3005	.2947	.2880	.2700
5		0	270, 90	139.80	111.60	83.20	54.60	26.10	.5592	.5580	.5547	.5460	.5220
19		8	90	82.70	65.30	49.20	32.50	15.40	.3308	.3265	.3280	.3250	.3080
30		32	90	3.50	2.73	1.79	1.02	.79	.0140	.0137	.0119	.0102	.0158
20		16	315	47.90	37.80	27.60	17.60	8.30	.1916	.1890	.1840	.1760	.1660
5		0	315, 135	139.80	111.60	83.20	54.60	26.10	.5592	.5580	.5547	.5460	.5220
17		16	135	4.92	3.60	3.55	2.11	.10	.0197	.0180	.0237	.0211	.0020

TABLE I.- SURFACE PRESSURE DATA RESULTS OF M_j = 1.0 NOZZLE EXHAUST PLUME IMPINGING UPON AN AXIALLY PARALLEL ADJACENT PLATE - Continued

(c) $\frac{y}{d_j} = \frac{3.750}{0.125} = 30$

				1	2	3	4	5	6	7	8	9	10
Orifice	$\frac{x}{d_j}$	$\frac{R}{d_j}$	ψ, deg	p_s/p_∞ for values of $p_{t,j}/p_\infty$ of -					$p_s/p_{t,j}$ for values of $p_{t,j}/p_\infty$ of -				
				250,000	200,000	150,000	100,000	50,000	250,000	200,000	150,000	100,000	50,000
1	-4	16	180	7.90	6.10	2.41	0.27	0.79	0.0316×10^{-3}	0.0305×10^{-3}	0.0161×10^{-3}	0.0027×10^{-3}	0.0158×10^{-3}
2	0	12		8.02	6.21	5.35	2.75	.70	.0321	.0311	.0357	.0275	.0140
3	4	8		16.15	14.20	10.94	4.80	2.85	.0646	.0710	.0729	.0480	.0570
4	8	4		26.13	21.50	14.90	9.85	10.75	.1045	.1075	.0993	.0985	.2150
5	12	0	180, 0	30.60	24.35	18.00	12.35	5.97	.1224	.1218	.1200	.1235	.1194
6	16	4	0	36.90	29.25	21.80	13.60	6.70	.1476	.1463	.1453	.1360	.1340
7	20	8		39.05	30.90	22.80	14.40	7.02	.1562	.1545	.1520	.1440	.1404
8	28	16		32.00	25.35	18.70	12.53	6.45	.1280	.1268	.1247	.1253	.1290
9	36	24		24.38	18.70	13.10	7.50	4.35	.0975	.0935	.0873	.0750	.0870
10	44	32		17.11	13.31	9.50	5.74	3.11	.0684	.0666	.0633	.0574	.0622
11	60	48		8.40	6.66	4.92	3.20	1.74	.0336	.0333	.0328	.0320	.0348
12	76	64		5.02	3.85	2.68	1.53	.90	.0201	.0193	.0179	.0153	.0180
13	108	96		1.18	1.14	1.00	.59	.37	.0047	.0057	.0067	.0059	.0074
14	140	128		.71	.64	.58	.51	.61	.0028	.0032	.0039	.0051	.0122
15	172	160		.91	.85	.75	.58	.75	.0036	.0043	.0050	.0058	.0150
5		0	22.5	30.60	24.35	18.00	12.35	5.97	.1224	.1218	.1200	.1235	.1194
28		72		2.83	2.40	1.78	1.10	.63	.0113	.0120	.0119	.0110	.0126
27		136		.76	.61	.45	.57	.67	.0030	.0031	.0030	.0057	.0134
16		16	225	7.90	6.21	7.41	3.75	.76	.0316	.0311	.0494	.0375	.0152
5		0	225, 45	30.60	24.35	18.00	12.35	5.97	.1224	.1218	.1200	.1235	.1194
21		16	45	29.26	22.50	16.22	9.83	5.20	.1170	.1125	.1081	.0983	.1040
22		48		7.30	5.66	4.04	2.41	1.42	.0292	.0283	.0269	.0241	.0284
23		84		1.67	1.45	1.14	.67	.50	.0067	.0073	.0076	.0067	.0100
24		112		.88	.71	.53	.35	.49	.0035	.0036	.0035	.0035	.0098
25		144		.70	.65	.61	.48	.81	.0028	.0033	.0040	.0048	.0162
26		176		.90	.70	.46	-----	.85	.0036	.0035	.0031	------	.0170
5		0	67.5	30.60	24.35	18.00	12.35	5.97	.1224	.1218	.1200	.1235	.1194
29		72	67.5	2.05	1.64	1.17	.47	1.05	.0082	.0082	.0078	.0047	.0210
18		8	270	27.85	22.28	16.60	12.33	5.52	.1114	.1114	.1107	.1233	.1104
5		0	270, 90	30.60	24.35	18.00	12.35	5.97	.1224	.1218	.1200	.1235	.1194
19		8	90	26.98	21.63	16.20	11.65	5.40	.1079	.1082	.1080	.1165	.1080
30		32	90	6.42	4.96	3.51	2.25	1.96	.0257	.0248	.0234	.0225	.0392
20		16	315	30.93	23.93	17.38	10.82	5.60	.1237	.1197	.1159	.1082	.1120
5		0	315, 135	30.60	24.35	18.00	12.35	5.97	.1224	.1218	.1200	.1235	.1194
17		16	135	8.28	6.43	5.89	8.10	.85	.0331	.0322	.0393	.0810	.0170

TABLE I.- SURFACE PRESSURE DATA RESULTS OF $M_j = 1.0$ NOZZLE EXHAUST PLUME IMPINGING UPON AN AXIALLY PARALLEL ADJACENT PLATE - Concluded

(d) $\frac{y}{d_j} = \frac{7.500}{0.125} = 60$

				1	2	3	4	5	6	7	8	9	10
Orifice	$\frac{x}{d_j}$	$\frac{R}{d_j}$	ψ, deg	p_s/p_∞ for values of $p_{t,j}/p_\infty$ of -					$p_s/p_{t,j}$ for values of $p_{t,j}/p_\infty$ of -				
				250,000	200,000	150,000	100,000	50,000	250,000	200,000	150,000	100,000	50,000
1	10	16	180	----	9.10	2.10	0.58	0.62	-------------	0.0455×10^{-3}	0.0140×10^{-3}	0.0058×10^{-3}	0.0124×10^{-3}
2	14	12		----	16.45	3.65	.53	----	-------------	.0823	.0243	.0053	------
3	18	8		5.80	4.55	12.25	3.21	.20	0.0232×10^{-3}	.0228	.0817	.0321	.0040
4	22	4		7.00	5.50	7.50	6.97	.83	.0280	.0275	.0500	.0697	.0166
5	26	0	180, 0	6.75	5.15	3.65	7.26	.96	.0270	.0258	.0244	.0726	.0192
6	30	4	0	7.00	5.50	4.10	6.25	1.63	.0280	.0275	.0273	.0625	.0326
7	34	8		7.20	5.75	4.30	3.45	1.90	.0288	.0288	.0287	.0345	.0380
8	42	16		7.10	5.61	4.20	2.90	2.62	.0284	.0280	.0280	.0290	.0524
9	50	24		6.85	5.30	3.40	1.70	1.20	.0274	.0265	.0227	.0170	.0240
10	58	32		6.55	4.90	3.45	2.06	1.10	.0262	.0245	.0230	.0206	.0220
11	74	48		4.85	3.90	2.95	1.95	.96	.0194	.0195	.0197	.0195	.0192
12	90	64		3.75	2.90	2.10	1.35	.55	.0150	.0145	.0140	.0135	.0110
13	122	96		1.60	1.39	1.15	.76	.36	.0064	.0070	.0077	.0076	.0072
14	154	128		.97	.82	.69	.57	.46	.0039	.0041	.0046	.0057	.0092
15	186	160		1.28	1.10	.92	.74	.44	.0051	.0055	.0061	.0074	.0088
5		0	22.5	6.75	5.15	3.65	7.26	.96	.0270	.0258	.0244	.0726	.0192
28		72		2.93	2.35	1.73	1.03	.46	.0117	.0118	.0115	.0103	.0092
27		136		1.27	.97	.67	.61	.48	.0051	.0049	.0045	.0061	.0096
16		16	225	7.21	15.90	4.15	.72	.45	.0288	.0795	.0277	.0072	.0090
5		0	225, 45	6.75	5.15	3.65	7.26	.96	.0270	.0258	.0244	.0226	.0192
21		16	45	6.36	4.96	3.52	2.07	1.02	.0254	.0248	.0235	.0207	.0204
22		48		4.58	3.44	2.30	1.18	.90	.0183	.0172	.0153	.0118	.0180
23		84		1.74	1.50	1.20	.95	.90	.0070	.0075	.0080	.0095	.0180
24		112		1.08	.87	.66	.65	.61	.0043	.0044	.0044	.0065	.0122
25		144		.67	.64	.60	.72	.80	.0027	.0032	.0040	.0072	.0160
26		176		1.29	1.04	.79	.61	.52	.0052	.0052	.0053	.0061	.0104
5		0	67.5	6.75	5.15	3.65	7.26	.96	.0270	.0258	.0244	.0726	.0192
29		72	67.5	2.62	2.15	1.72	1.60	.30	.0105	.0108	.0115	.0160	.0060
18		8	270	6.93	5.46	3.85	5.13	.59	.0277	.0273	.0257	.0513	.0118
5		0	270, 90	6.75	5.15	3.65	7.26	.96	.0270	.0258	.0244	.0726	.0192
19		8	90	6.53	5.11	4.05	3.81	.50	.0261	.0256	.0270	.0381	.0100
30		32	90	3.95	4.11	7.23	2.10	.80	.0158	.0206	.0482	.0210	.0160
20		16	315	6.85	5.40	3.94	2.45	2.73	.0274	.0270	.0263	.0245	.0546
5		0	315, 135	6.75	5.15	3.65	7.26	.96	.0270	.0258	.0244	.0726	.0192
17		16	135	7.21	20.50	3.43	.83	.45	.0288	.1025	.0229	.0083	.0090

TABLE II.- SURFACE PRESSURE DATA RESULTS OF $M_j = 5.0$ NOZZLE EXHAUST PLUME IMPINGING UPON AN AXIALLY PARALLEL ADJACENT PLATE

(a) $\frac{y}{d_j} = \frac{1.250}{0.625} = 2$

				1	2	3	4	5	6	7	8	9	10
Orifice	$\frac{x}{d_j}$	$\frac{R}{d_j}$	ψ, deg	p_s/p_∞ for values of $p_{t,j}/p_\infty$ of -					$p_s/p_{t,j}$ for values of $p_{t,j}/p_\infty$ of -				
				250,000	200,000	150,000	100,000	50,000	250,000	200,000	150,000	100,000	50,000
1	0	3.2	180	1.00	0.83	0.79	0.75	0.61	0.0040×10^{-3}	0.0042×10^{-3}	0.0053×10^{-3}	0.0075×10^{-3}	0.0122×10^{-3}
2	.8	2.4		9.58	6.22	8.12	.36	-----	.0383	.0311	.0541	.0036	------
3	1.6	1.6		57.80	53.10	36.80	19.90	11.90	.2312	.2655	.2453	.1990	.2380
4	2.4	.8		130.60	92.40	76.00	56.80	23.10	.5224	.4620	.5067	.5680	.4620
5	3.2	0	180, 0	113.00	90.40	66.10	43.80	21.50	.4520	.4520	.4407	.4380	.4300
6	4.0	.8	0	95.30	76.70	56.90	37.30	18.40	.3312	.3835	.3793	.3730	.3680
7	4.8	1.6		74.20	59.90	44.40	28.50	14.00	.2968	.2995	.2960	.2850	.2800
8	6.4	3.2		44.30	35.10	26.10	17.10	8.50	.1772	.1755	.1740	.1710	.1700
9	8.0	4.8		27.90	21.40	14.20	8.80	3.50	.1116	.1070	.0947	.0880	.0700
10	9.6	6.4		17.80	13.80	9.80	6.00	2.60	.0712	.0690	.0653	.0600	.0520
11	12.8	9.6		9.25	7.31	5.40	3.50	1.68	.0370	.0366	.0360	.0350	.0336
12	16.0	12.8		4.74	3.93	2.83	1.63	.67	.0190	.0197	.0189	.0163	.0134
13	22.4	19.2		1.57	1.47	1.19	.75	.37	.0063	.0074	.0079	.0075	.0074
14	28.8	25.6		1.00	.83	.66	.49	.49	.0040	.0042	.0044	.0049	.0098
15	35.2	32.0		.97	.81	.79	.63	.26	.0039	.0041	.0053	.0063	.0052
5		0	22.5	113.00	90.40	66.10	43.80	21.50	.4520	.4520	.4407	.4380	.4300
28		14.4		2.00	1.91	1.41	.80	.29	.0080	.0096	.0094	.0080	.0058
27		27.2		.77	.67	.63	.61	.40	.0031	.0034	.0042	.0061	.0080
16		3.2	225	2.40	2.04	1.15	.32	.52	.0096	.0102	.0077	.0032	.0104
5		0	225, 45	113.00	90.40	66.10	43.80	21.50	.4520	.4520	.4407	.4380	.4300
21		3.2	45	26.40	20.30	14.20	9.10	5.10	.1056	.1015	.0947	.0910	.1020
22		9.6		2.02	1.92	1.26	.88	.38	.0081	.0096	.0084	.0088	.0076
23		16.8		.76	.62	.50	.56	.45	.0030	.0031	.0033	.0056	.0090
24		22.4		.87	.70	.53	.86	.53	.0035	.0035	.0035	.0086	.0106
25		28.8		.75	.66	.91	.86	.79	.0030	.0033	.0061	.0086	.0158
26		35.2		.84	.77	.49	.18	.15	.0034	.0039	.0033	.0018	.0030
5		0	67.5	113.00	90.40	66.10	43.80	21.50	.4520	.4520	.4407	.4380	.4300
29		14.4	67.5	.85	.76	.91	.69	.23	.0034	.0038	.0061	.0069	.0046
18		1.6	270	49.80	36.00	26.80	20.20	7.20	.1992	.1800	.1787	.2020	.1440
5		0	270, 90	113.00	90.40	66.10	43.80	21.50	.4520	.4520	.4407	.4380	.4300
19		1.6	90	44.00	32.30	24.40	18.00	6.20	.1760	.1615	.1627	.1800	.1240
30		6.4	90	.78	.77	.72	.85	.51	.0031	.0039	.0048	.0085	.0102
20		3.2	315	28.20	22.00	15.80	9.90	4.70	.1128	.1100	.1053	.0990	.0940
5		0	315, 135	113.00	90.40	66.10	43.80	21.50	.4520	.4520	.4407	.4380	.4300
17		3.2	135	2.19	1.85	.86	.39	.57	.0088	.0093	.0057	.0039	.0114

TABLE II.- SURFACE PRESSURE DATA RESULTS OF $M_j = 5.0$ NOZZLE EXHAUST PLUME IMPINGING UPON AN AXIALLY PARALLEL ADJACENT PLATE - Continued

(b) $\frac{y}{d_j} = \frac{2.500}{0.625} = 4$

Orifice	$\frac{x}{d_j}$	$\frac{R}{d_j}$	ψ, deg	p_s/p_∞ for values of $p_{t,j}/p_\infty$ of -					$p_s/p_{t,j}$ for values of $p_{t,j}/p_\infty$ of -				
				(1) 250,000	(2) 200,000	(3) 150,000	(4) 100,000	(5) 50,000	(6) 250,000	(7) 200,000	(8) 150,000	(9) 100,000	(10) 50,000
1	1.28	3.2	180	0.32	0.57	0.78	0.80	0.72	0.0013×10^{-3}	0.0029×10^{-3}	0.0052×10^{-3}	0.0080×10^{-3}	0.0144×10^{-3}
2	2.08	2.4		5.18	1.53	.60	.48	.60	.0207	.0077	.0040	.0048	.0120
3	2.88	1.6		16.18	10.05	12.15	5.00	.34	.0647	.0503	.0810	.0500	.0068
4	3.68	.8		21.50	19.61	15.57	8.94	3.68	.0860	.0981	.1038	.0894	.0736
5	4.48	0	180, 0	25.35	21.62	17.22	11.82	8.65	.1014	.1081	.1148	.1182	.1730
6	5.28	.8	0	31.61	23.29	17.52	11.37	5.28	.1264	.1165	.1168	.1137	.1056
7	6.08	1.6		34.07	25.88	18.12	11.70	5.30	.1363	.1294	.1208	.1170	.1060
8	7.68	3.2		29.35	23.45	17.33	11.35	5.40	.1174	.1173	.1155	.1135	.1080
9	9.28	4.8		19.08	15.13	11.20	7.28	3.35	.0763	.0757	.0747	.0728	.0670
10	11.48	6.4		14.85	11.67	8.54	5.22	2.20	.0594	.0584	.0569	.0522	.0440
11	14.08	9.6		8.75	6.83	4.95	3.05	1.22	.0350	.0342	.0330	.0305	.0244
12	17.28	12.8		5.75	4.47	3.20	1.93	.80	.0230	.0224	.0213	.0193	.0160
13	23.68	19.2		2.10	1.85	1.35	.85	.35	.0084	.0093	.0090	.0085	.0070
14	30.08	25.6		1.20	1.10	.70	.55	.30	.0048	.0055	.0047	.0055	.0060
15	36.48	32.0		.95	.85	.70	.65	.50	.0038	.0043	.0047	.0065	.0100
5		0	22.5	25.35	21.62	17.22	11.82	8.65	.1014	.1081	.1148	.1182	.1730
28		14.4		2.86	2.40	1.77	1.15	.55	.0114	.0120	.0118	.0115	.0110
27		27.2		.75	.61	.45	.45	.37	.0030	.0031	.0030	.0045	.0074
16		3.2	225	.86	.60	.36	.22	.30	.0034	.0030	.0024	.0022	.0060
5		0	225, 45	25.35	21.62	17.22	11.82	8.65	.1014	.1081	.1148	.1182	.1730
21		3.2	45	19.85	13.67	8.92	5.14	1.64	.0794	.0684	.0595	.0514	.0328
22		9.6		3.17	2.25	1.22	.58	.67	.0127	.0112	.0081	.0058	.0134
23		16.8		.97	.77	.60	.73	.80	.0039	.0038	.0040	.0073	.0160
24		22.4		.71	.64	.60	.94	.75	.0028	.0032	.0040	.0094	.0150
25		28.8		1.00	1.00	1.00	.86	.75	.0040	.0050	.0067	.0086	.0150
26		35.2		1.00	.92	.88	.81	.71	.0040	.0046	.0059	.0081	.0142
5		0	67.5	25.35	21.62	17.22	11.82	8.65	.1014	.1081	.1148	.1182	.1730
29		14.4	67.5	.74	.73	.82	.78	.68	.0030	.0036	.0055	.0078	.0136
18		1.6	270	15.67	14.55	12.40	8.25	7.10	.0627	.0728	.0827	.0825	.1420
5		0	270, 90	25.35	21.62	17.22	11.82	8.65	.1014	.1081	.1148	.1182	.1730
19		1.6	90	16.30	15.55	12.56	8.75	9.72	.0652	.0778	.0837	.0875	.1944
30		6.4	90	1.49	.74	.60	.57	.40	.0060	.0037	.0040	.0057	.0080
20		3.2	315	20.25	15.74	10.90	7.34	3.75	.0810	.0787	.0727	.0734	.0750
5		0	315, 135	25.35	21.62	17.22	11.82	8.65	.1014	.1081	.1148	.1182	.1730
17		3.2	135	1.30	1.12	.96	.80	.66	.0052	.0056	.0064	.0080	.0132

TABLE II.- SURFACE PRESSURE DATA RESULTS OF $M_j = 5.0$ NOZZLE EXHAUST PLUME IMPINGING UPON AN AXIALLY PARALLEL ADJACENT PLATE - Continued

(c) $\frac{y}{d_j} = \frac{3.750}{0.625} = 6$

Orifice	$\frac{x}{d_j}$	$\frac{R}{d_j}$	ψ, deg	(1) p_s/p_∞ for values of $p_{t,j}/p_\infty$ of -	(2)	(3)	(4)	(5)	(6) $p_s/p_{t,j}$ for values of $p_{t,j}/p_\infty$ of -	(7)	(8)	(9)	(10)
				250,000	200,000	150,000	100,000	50,000	250,000	200,000	150,000	100,000	50,000
1	3.2	3.2	180	0.72	0.70	0.71	0.62	0.46	0.0029×10^{-3}	0.0035×10^{-3}	0.0047×10^{-3}	0.0062×10^{-3}	0.0092×10^{-3}
2	4.0	2.4	↓	2.14	.78	.22	.13	----	.0086	.0039	.0015	.0013	------
3	4.8	1.6		6.55	13.60	.81	----	----	.0262	.0680	.0054	------	------
4	5.6	.8		11.06	8.50	25.85	2.50	.50	.0442	.0425	.1723	.0250	.0100
5	6.4	0	180, 0	11.46	8.70	4.95	9.93	----	.0458	.0435	.0330	.0993	------
6	7.2	.8	0	13.15	10.71	7.37	5.12	2.18	.0526	.0536	.0491	.0512	.0436
7	8.0	1.6		14.83	11.50	8.50	4.75	5.60	.0593	.0575	.0567	.0475	.1120
8	9.6	3.2		13.63	10.69	7.82	5.02	3.17	.0545	.0535	.0521	.0502	.0634
9	11.2	4.8		11.47	8.75	5.58	2.85	.50	.0459	.0438	.0372	.0285	.0100
10	12.8	6.4		10.18	7.60	5.18	2.95	.95	.0407	.0380	.0345	.0295	.0190
11	16.0	9.6		7.32	5.80	4.25	2.72	1.30	.0293	.0290	.0283	.0272	.0260
12	19.2	12.8		5.52	4.23	2.94	1.72	.66	.0221	.0212	.0196	.0172	.0132
13	25.6	19.2		2.28	2.04	1.48	.90	.38	.0091	.0102	.0099	.0090	.0076
14	32.0	25.6		1.20	1.16	.88	.51	.28	.0048	.0058	.0057	.0051	.0056
15	38.4	32.0	↓	.98	.82	.64	.48	.07	.0039	.0041	.0043	.0048	.0014
5		0	22.5	11.46	8.70	4.95	9.93	----	.0458	.0435	.0330	.0993	------
28		14.4	↓	2.84	2.43	1.70	.94	.47	.0114	.0122	.0113	.0094	.0094
27		27.2		.74	.65	.49	.36	.70	.0030	.0033	.0033	.0036	.0140
16		3.2	225	1.21	.76	.64	.58	.42	.0048	.0038	.0043	.0058	.0084
5		0	225, 45	11.46	8.70	4.95	9.93	----	.0458	.0435	.0330	.0993	------
21		3.2	45	10.86	8.11	5.60	2.92	2.52	.0434	.0406	.0373	.0292	.0504
22		9.6		3.62	2.97	2.38	1.64	.81	.0145	.0148	.0159	.0164	.0162
23		16.8		1.15	1.15	1.11	.90	.62	.0046	.0058	.0074	.0090	.0124
24		22.4		.83	.76	.88	.60	.39	.0033	.0038	.0059	.0060	.0078
25		28.8		.74	.82	.95	.85	.81	.0030	.0041	.0063	.0085	.0162
26		35.2	↓	.85	.58	.14	----	----	.0034	.0029	.0009	------	------
5		0	67.5	11.46	8.70	4.95	9.93	----	.0458	.0435	.0330	.0993	------
29		14.4	67.5	.87	.82	.73	.53	----	.0035	.0041	.0049	.0053	------
18		1.6	270	11.84	8.11	4.38	7.68	----	.0474	.0406	.0292	.0767	------
5		0	270, 90	11.46	8.70	4.95	9.93	----	.0458	.0435	.0330	.0993	------
19		1.6	90	11.30	7.33	9.42	3.47	.16	.0452	.0366	.0628	.0347	.0032
30		6.4	90	.65	.73	.65	.64	.43	.0026	.0036	.0043	.0064	.0086
20		3.2	315	11.75	8.75	6.20	3.28	2.91	.0470	.0438	.0413	.0328	.0582
5		0	315, 135	11.46	8.70	4.95	9.92	----	.0458	.0435	.0330	.0993	------
17		3.2	135	1.44	.81	.64	.52	.48	.0058	.0040	.0043	.0052	.0096

TABLE II.- SURFACE PRESSURE DATA RESULTS OF $M_j = 5.0$ NOZZLE EXHAUST PLUME IMPINGING UPON AN AXIALLY PARALLEL ADJACENT PLATE - Concluded

(d) $\frac{y}{d_j} = \frac{6.250}{0.625} = 10$

Orifice	$\frac{x}{d_j}$	$\frac{R}{d_j}$	ψ, deg	p_s/p_∞ for values of $p_{t,j}/p_\infty$ of -					$p_s/p_{t,j}$ for values of $p_{t,j}/p_\infty$ of -				
				1	2	3	4	5	6	7	8	9	10
				250,000	200,000	150,000	100,000	50,000	250,000	200,000	150,000	100,000	50,000
1	8.0	3.2	180	0.93	0.94	0.95	0.96	0.79	0.0037×10^{-3}	0.0047×10^{-3}	0.0063×10^{-3}	0.0096×10^{-3}	0.0158×10^{-3}
2	8.8	2.4		1.09	.97	.85	.77	.70	.0044	.0049	.0057	.0077	.0140
3	9.6	1.6		11.85	2.88	.87	.68	.64	.0474	.0144	.0058	.0068	.0128
4	10.4	.8		22.00	7.44	2.31	.66	.59	.0880	.0372	.0154	.0066	.0118
5	11.2	0	180, 0	13.85	9.52	4.78	.68	.47	.0554	.0476	.0319	.0068	.0094
6	12.0	.8	0	4.22	9.77	6.83	1.13	.42	.0169	.0489	.0455	.0113	.0084
7	12.8	1.6		4.80	5.50	7.41	2.06	.31	.0192	.0275	.0494	.0206	.0062
8	14.4	3.2		4.91	4.34	3.97	3.73	.67	.0196	.0217	.0265	.0373	.0134
9	16.0	4.8		4.25	3.80	2.72	2.98	.71	.0170	.0190	.0181	.0298	.0142
10	17.6	6.4		4.50	3.91	2.61	2.13	.75	.0180	.0196	.0174	.0213	.0150
11	20.8	9.6		3.72	3.07	2.16	1.28	.83	.0149	.0154	.0144	.0128	.0166
12	24.0	12.8		2.86	2.45	1.79	1.05	.81	.0114	.0123	.0119	.0105	.0162
13	30.4	19.2		1.60	1.52	1.16	.66	.46	.0064	.0076	.0077	.0066	.0092
14	36.8	25.6		1.12	.91	.68	.42	.26	.0045	.0046	.0045	.0042	.0052
15	43.2	32.0		.81	.79	.76	.55	.35	.0032	.0040	.0051	.0055	.0070
5		0	22.5	13.85	9.52	4.78	.68	.47	.0554	.0476	.0319	.0068	.0094
28		14.4		2.32	1.98	1.51	1.18	.92	.0093	.0099	.0101	.0118	.0184
27		27.2		1.02	.82	.69	.75	.86	.0041	.0041	.0046	.0075	.0172
16		3.2	225	1.54	.72	.60	.38	.36	.0062	.0036	.0040	.0038	.0072
5		0	225, 45	13.85	9.52	4.78	.68	.47	.0554	.0476	.0319	.0068	.0094
21		3.2	45	3.43	3.67	5.38	.10	----	.0137	.0184	.0359	.0010	------
22		9.6		2.53	2.54	2.50	.87	.25	.0101	.0127	.0167	.0087	.0050
23		16.8		1.75	2.25	1.41	.97	.86	.0070	.0113	.0094	.0097	.0172
24		22.4		1.52	1.18	.94	.92	.82	.0061	.0059	.0063	.0092	.0164
25		28.8		.92	1.00	.88	.89	.79	.0037	.0050	.0059	.0089	.0158
26		35.2		-----	----	----	----	----	------	------	------	------	------
5		0	67.5	13.85	9.52	4.78	.68	.47	.0554	.0476	.0319	.0068	.0094
29		14.4	67.5	.96	1.00	1.00	.91	.73	.0038	.0050	.0067	.0091	.0146
18		1.6	270	13.10	8.73	3.64	1.11	.70	.0524	.0437	.0243	.0111	.0140
5		0	270, 90	13.85	9.52	4.78	.68	.47	.0554	.0476	.0319	.0068	.0094
19		1.6	90	12.88	8.31	2.83	.98	.68	.0515	.0416	.0189	.0098	.0136
30		6.4	90	1.08	1.00	.81	.68	.52	.0043	.0050	.0054	.0068	.0104
20		3.2	315	4.43	5.16	5.30	1.94	.79	.0177	.0258	.0353	.0194	.0158
5		0	315, 135	13.85	9.52	4.78	.68	.47	.0554	.0476	.0319	.0068	.0094
17		3.2	135	1.56	1.07	1.01	.88	.67	.0062	.0054	.0067	.0088	.0134

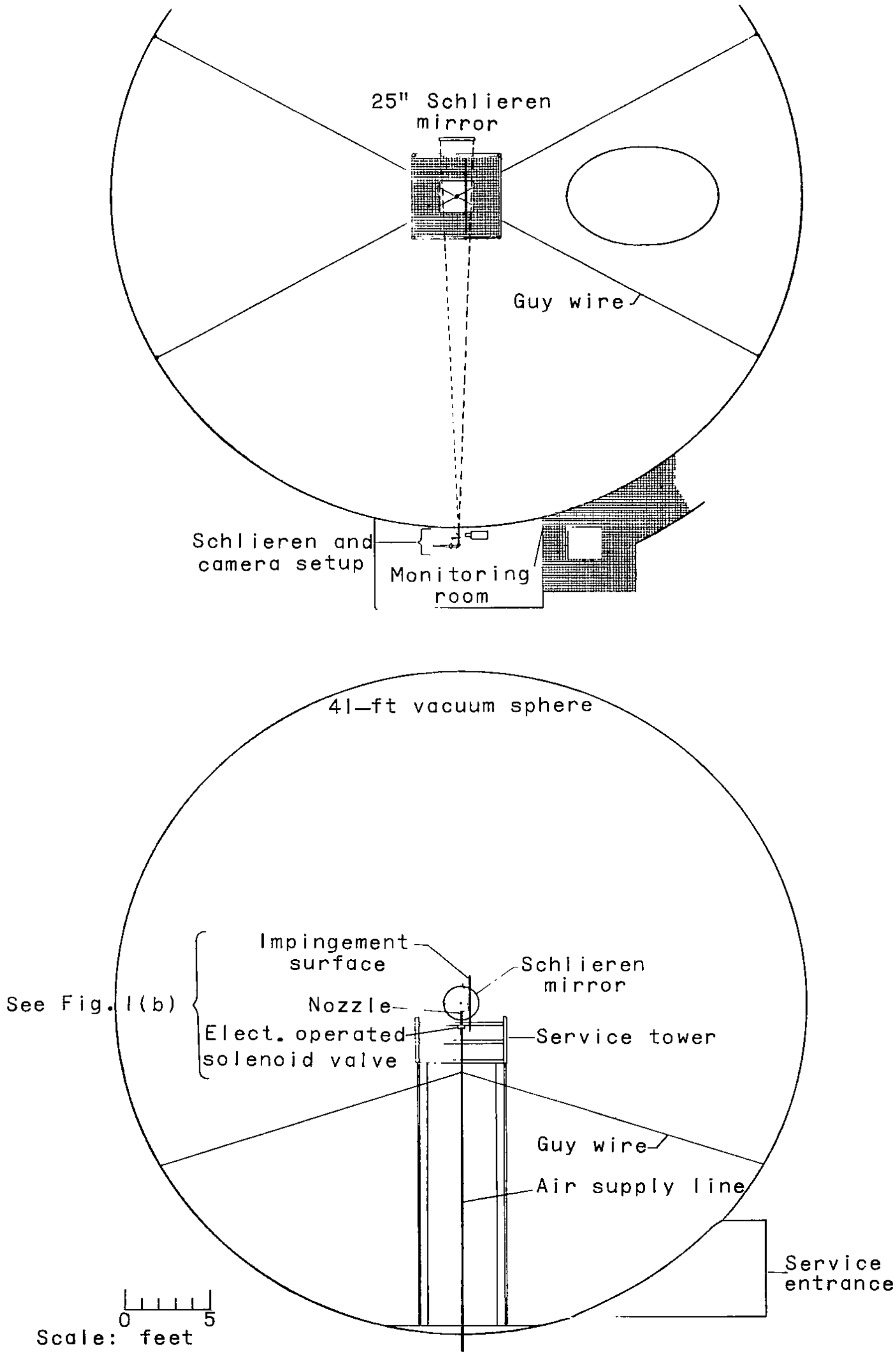

(a) Overall test setup.

Figure 1.- Sketches of test setup, nomenclature, and nozzles.

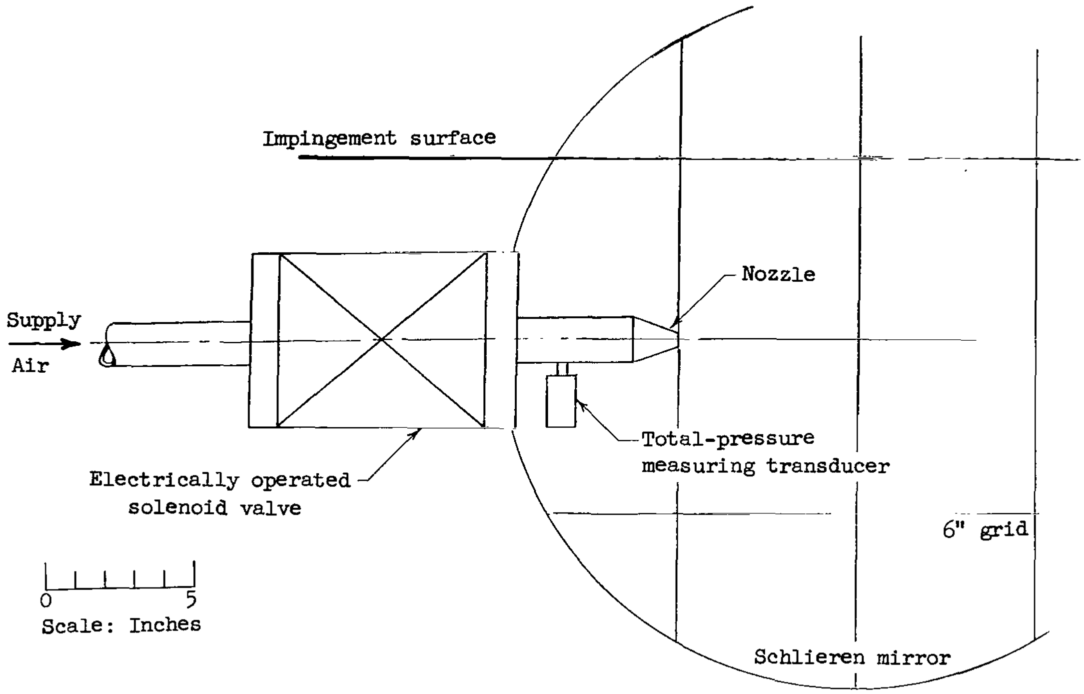

(b) Air supply apparatus.

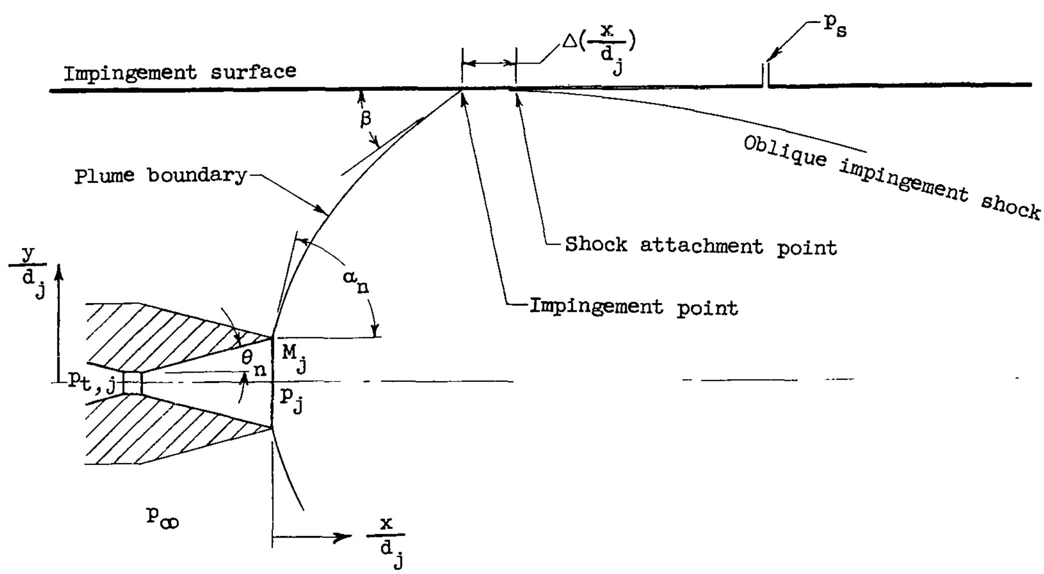

(c) Nomenclature sketch.

Figure 1.- Continued.

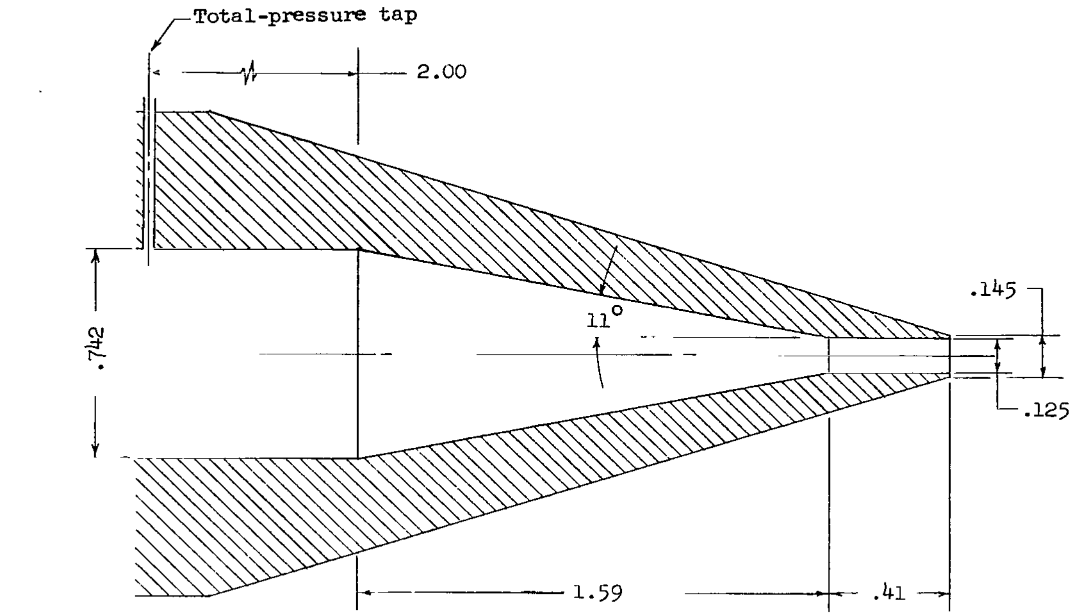

Convergent nozzle, $M_j = 1.0$.

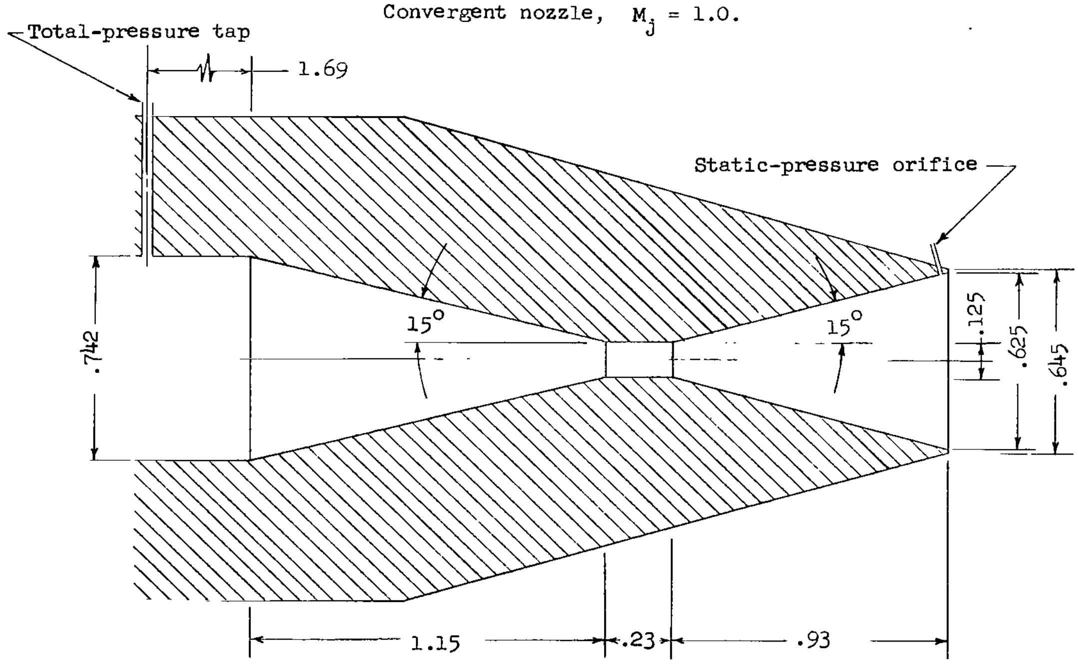

Convergent-divergent nozzle, $M_j = 5.0$.

(d) Test nozzles. All linear dimensions are in inches.

Figure 1.- Concluded.

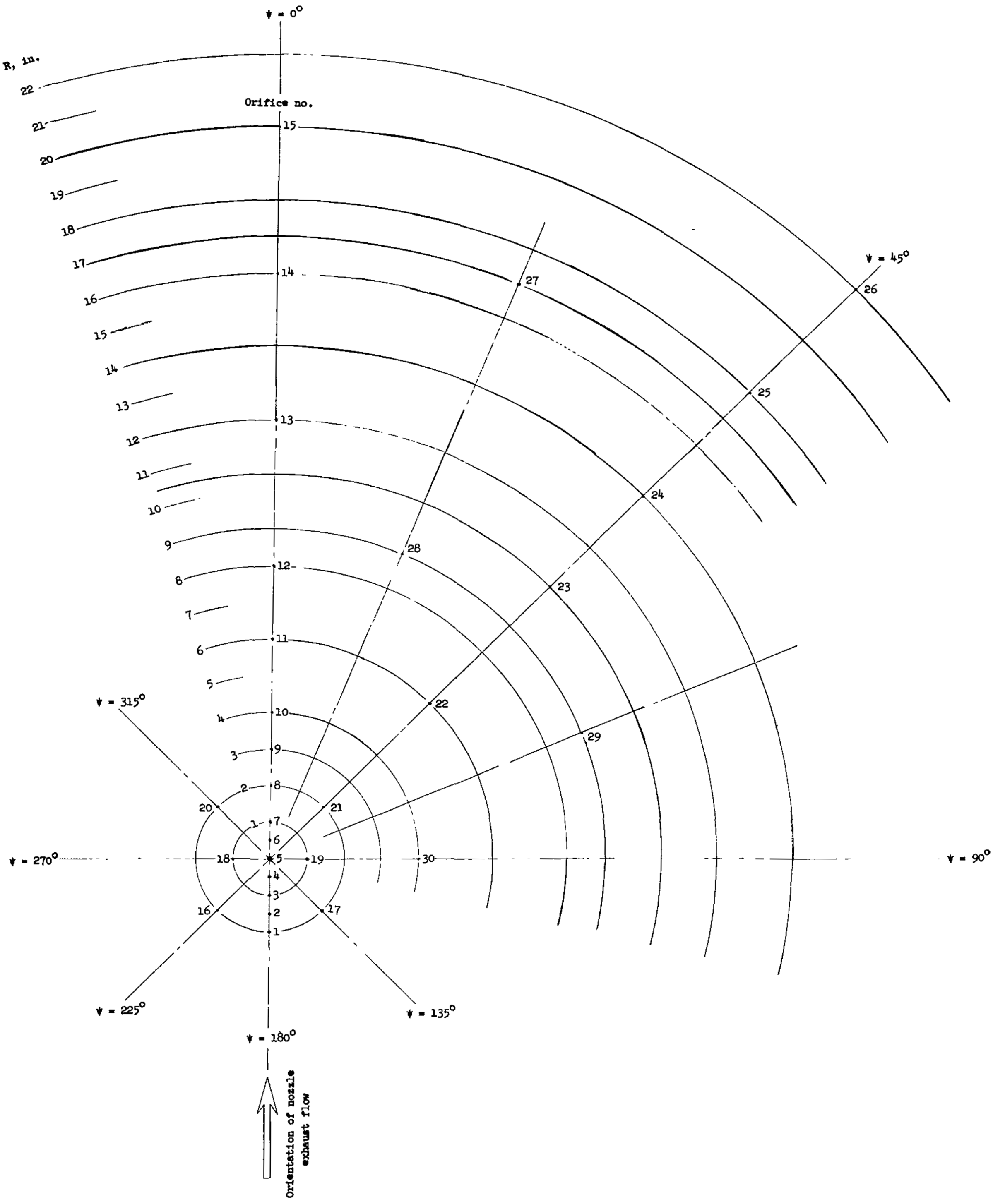

Figure 2.- Static-pressure orifice locations on impingement surface.

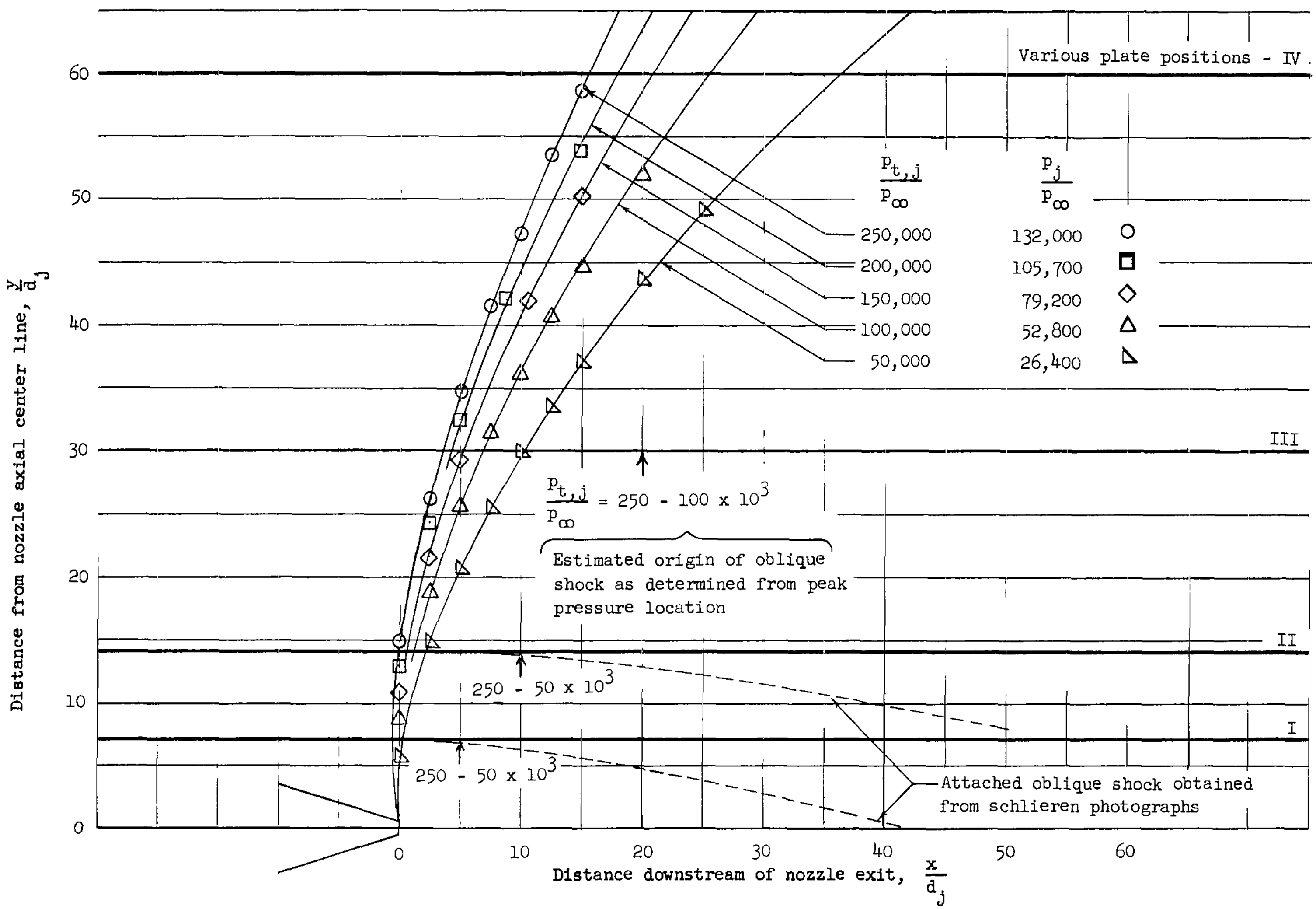

(a) $M_j = 1.0$; $d_j = 0.125$ in.

Figure 3.- Correlation of plate positions with jet exhaust plume boundaries for various ratios of jet total pressure to ambient pressure. Symbols indicate experimental points from photographs; solid lines indicate theoretically calculated jet plume boundaries.

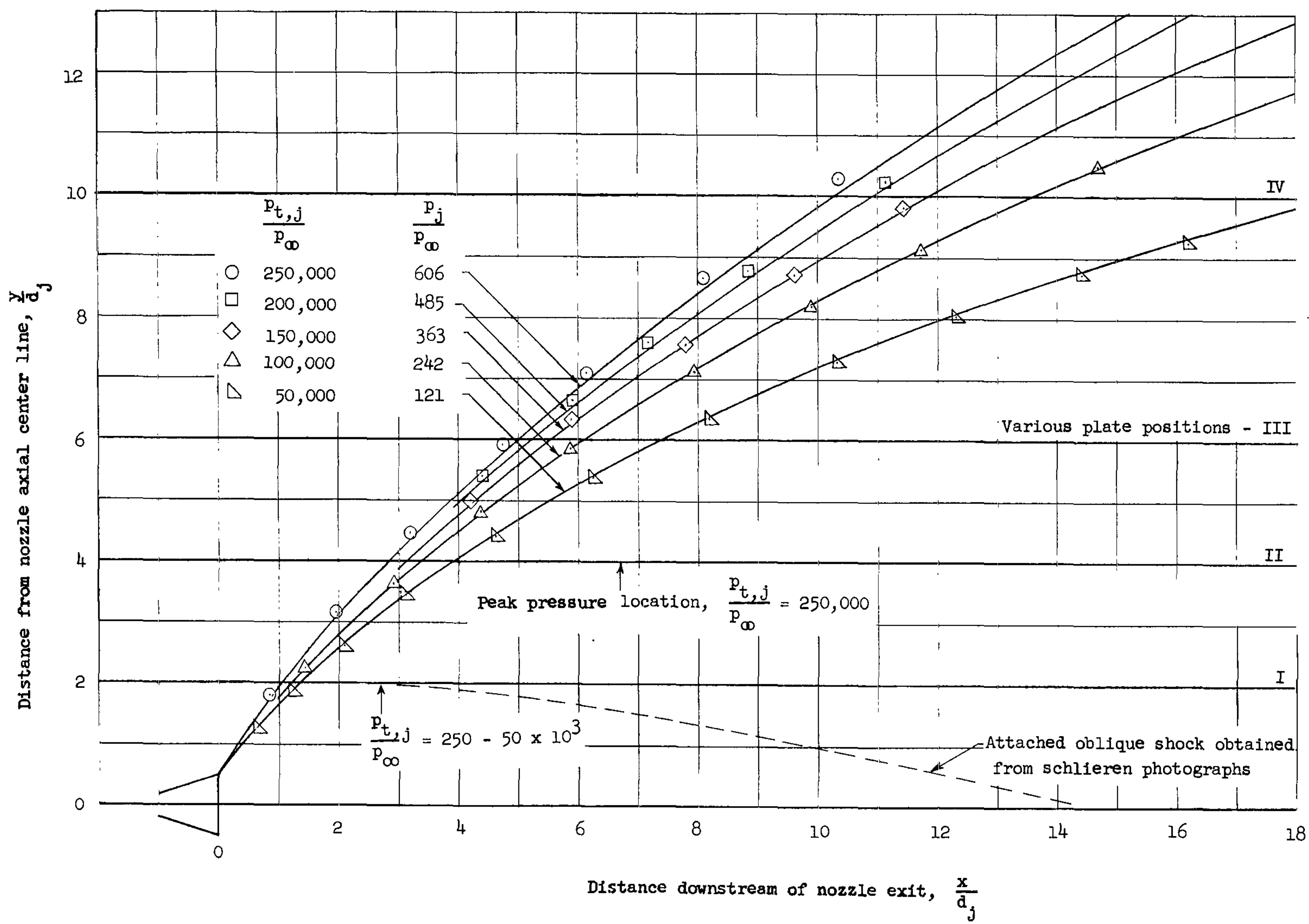

(b) $M_j = 5.0$; $d_j = 0.625$ in.

Figure 3.- Concluded.

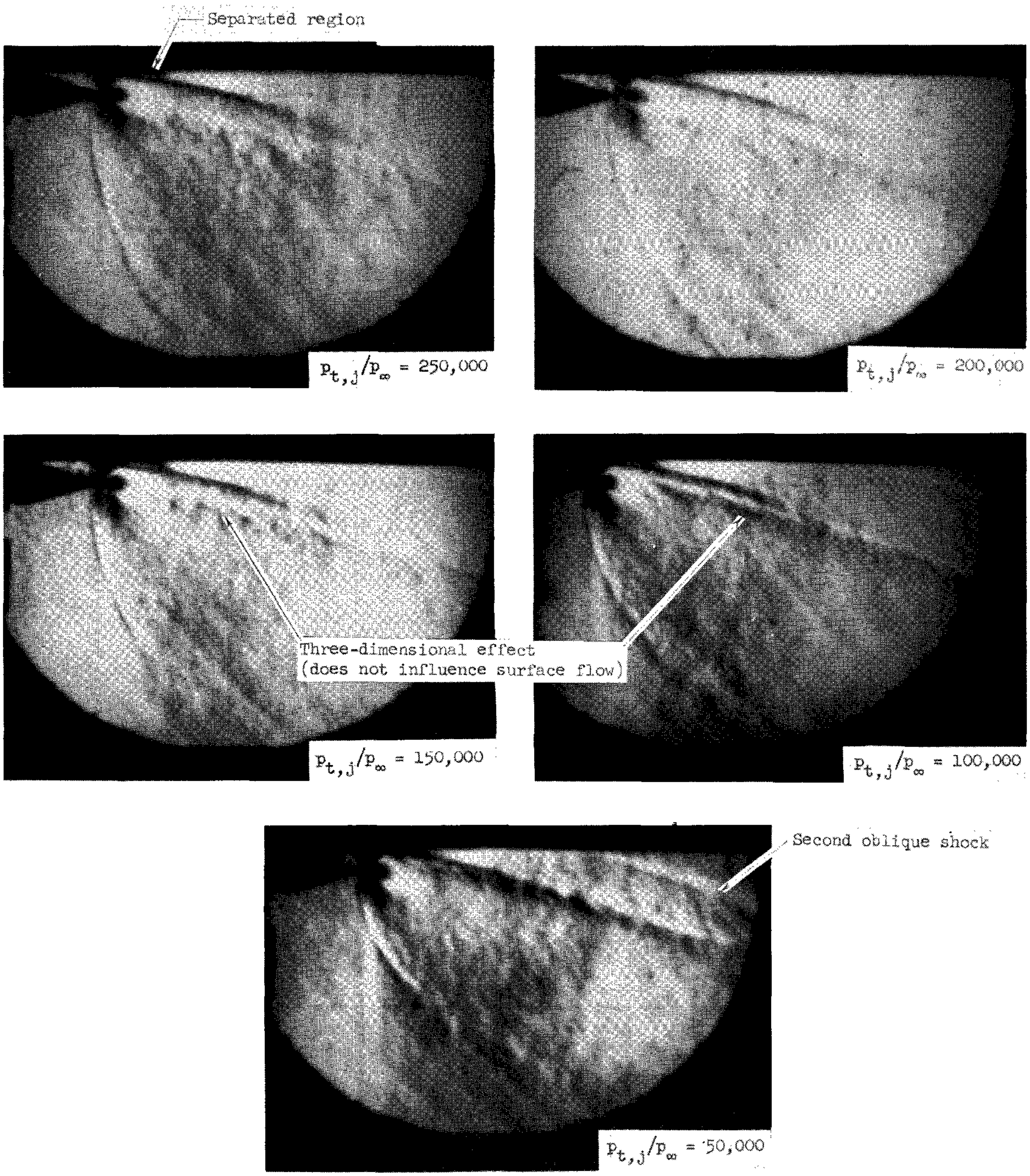

(a) $\frac{y}{d_j} = 7.$

Figure 4.- Jet plume schlieren photographs of $M_j = 1.0$ nozzle. L-64-383

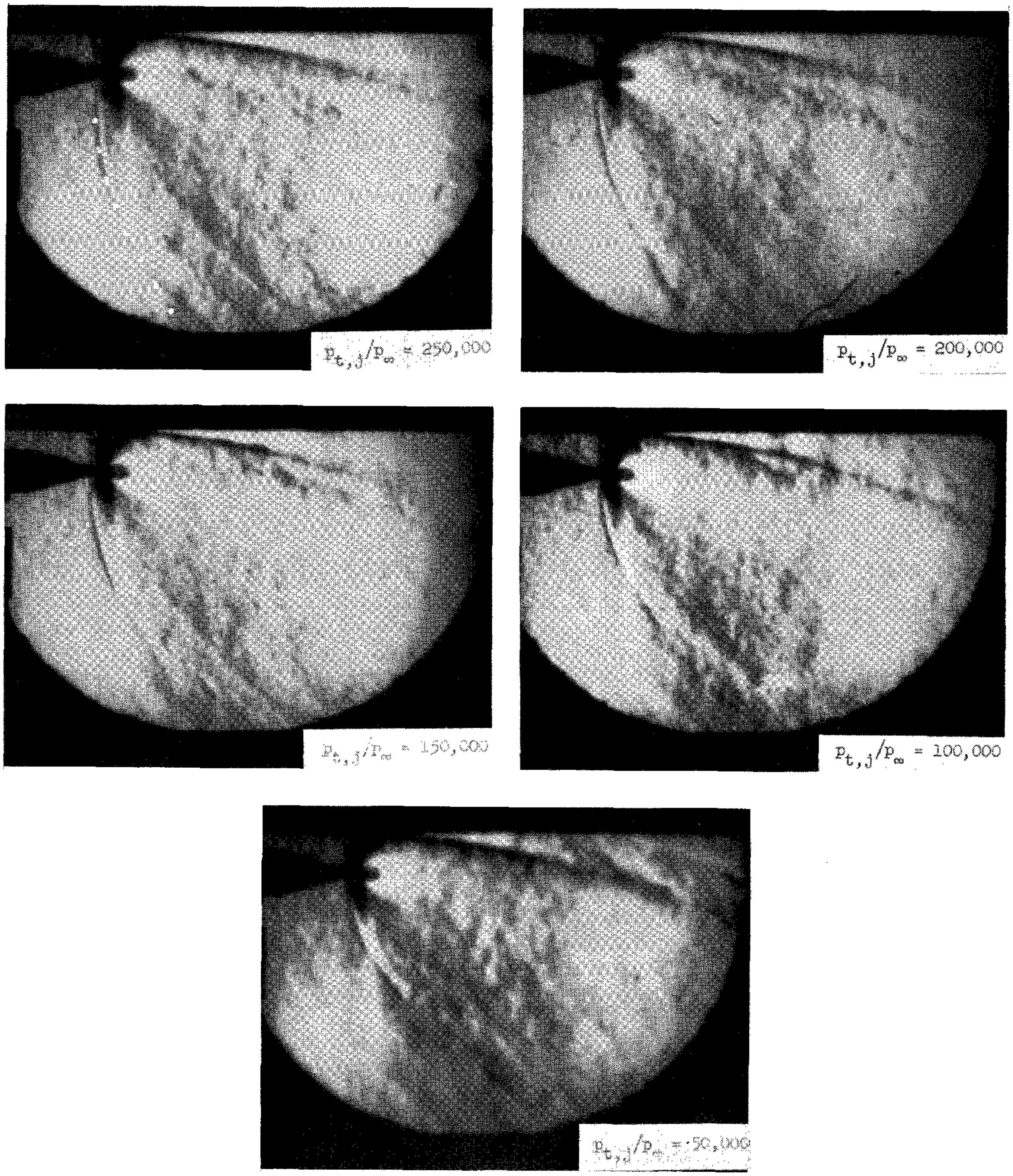

(b) $\frac{y}{d_j} = 14.$

Figure 4.- Continued. L-64-384

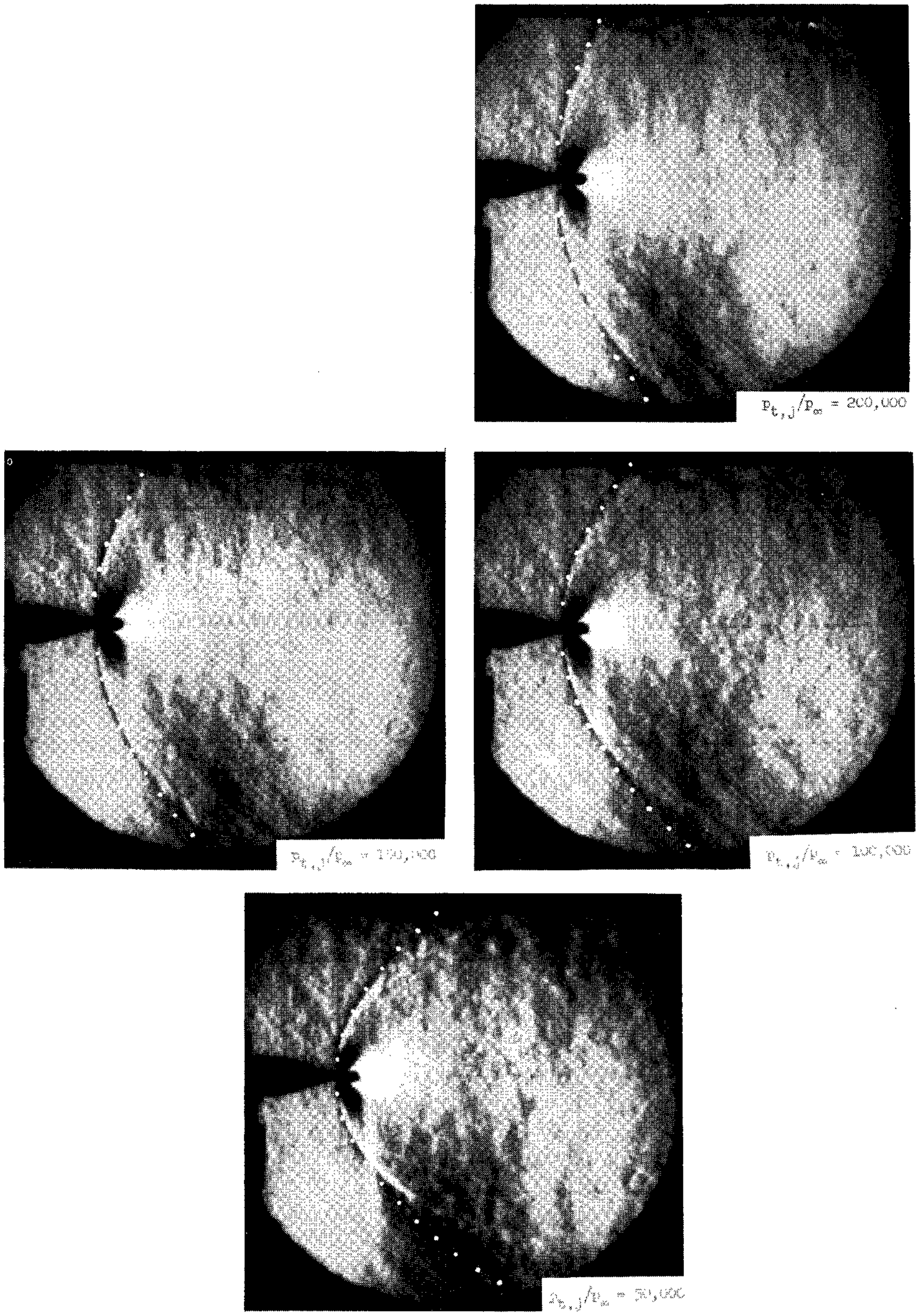

(c) $\dfrac{y}{d_j} = 60.$

Figure 4.- Concluded. L-64-385

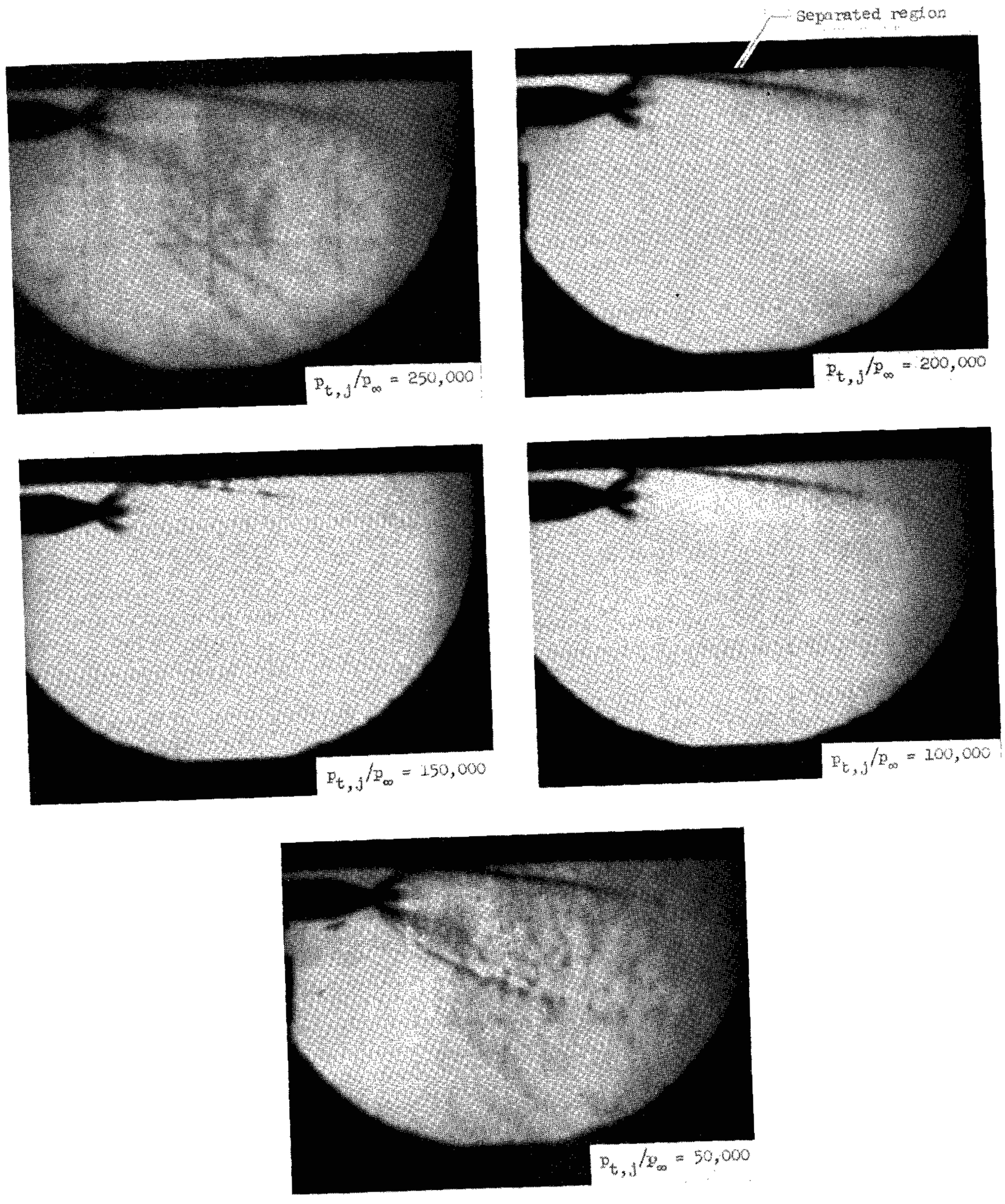

(a) $\frac{y}{d_j} = 2$.

Figure 5.- Jet plume schlieren photographs of $M_j = 5.0$ nozzle. L-64-386

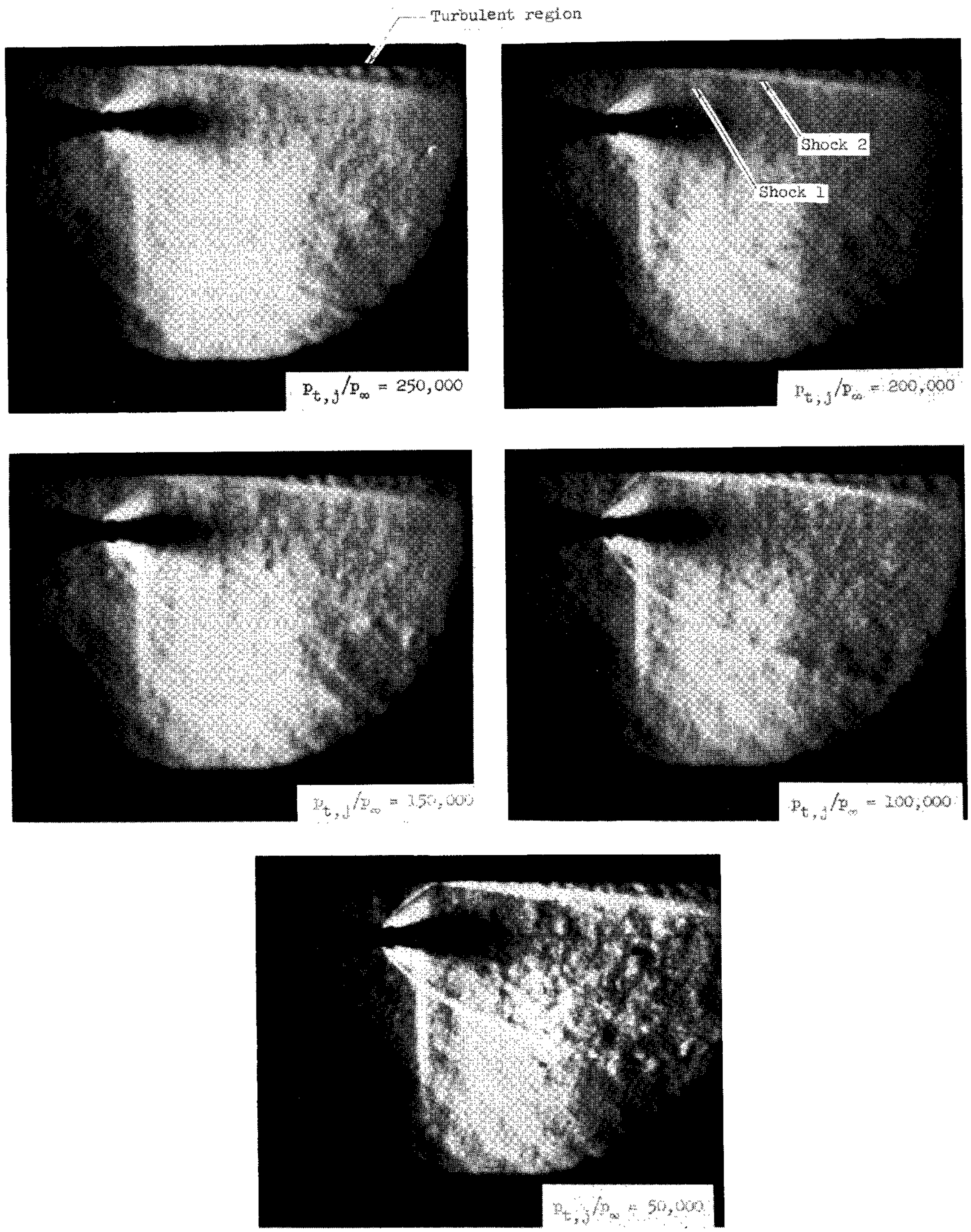

(b) $\frac{y}{d_j} = 4.$

Figure 5.- Continued.

L-64-387

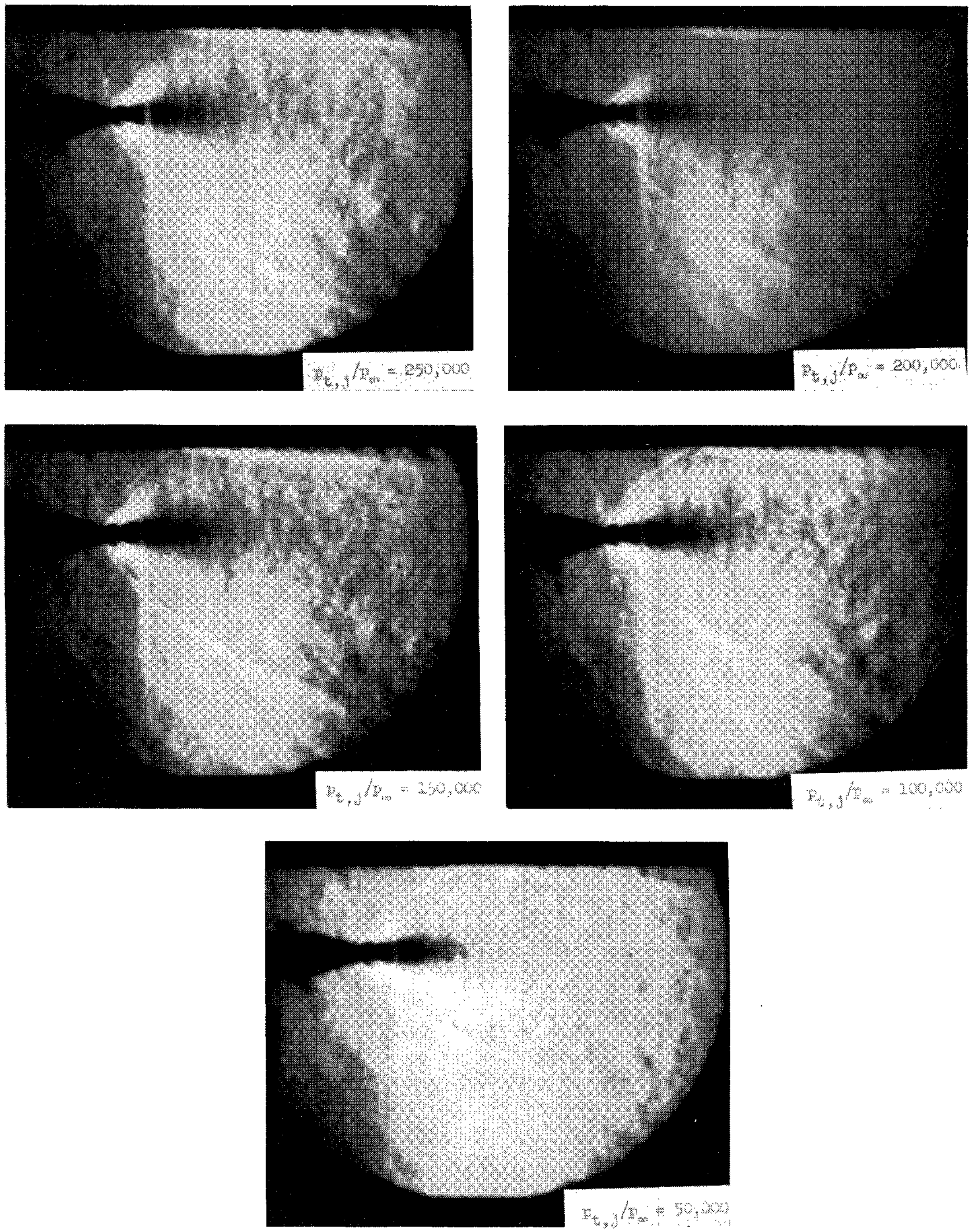

(c) $\frac{y}{d_j} = 6.$

Figure 5.- Continued. L-64-388

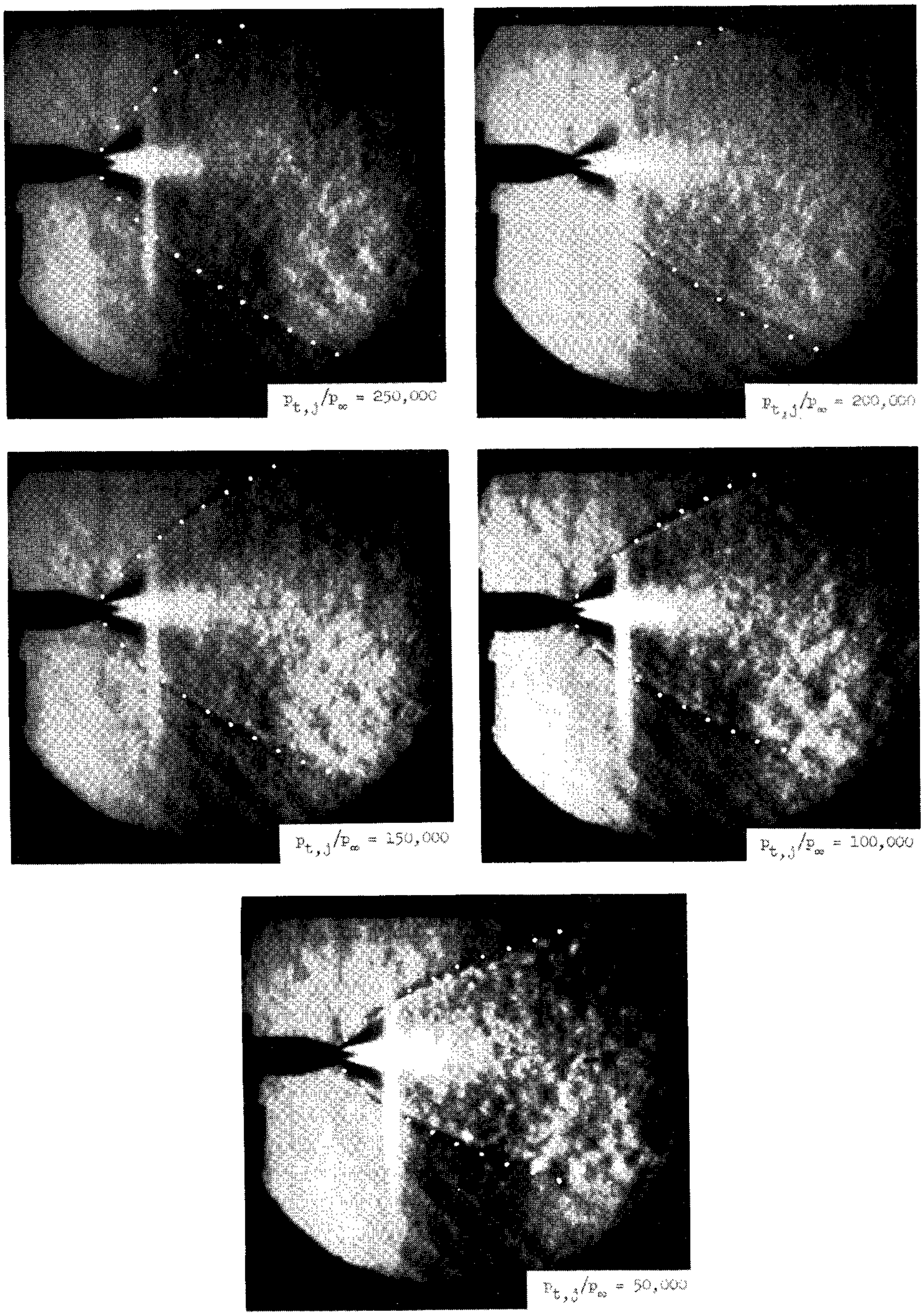

(d) $\frac{y}{d_j} = 10.$

Figure 5.- Concluded.

L-64-389

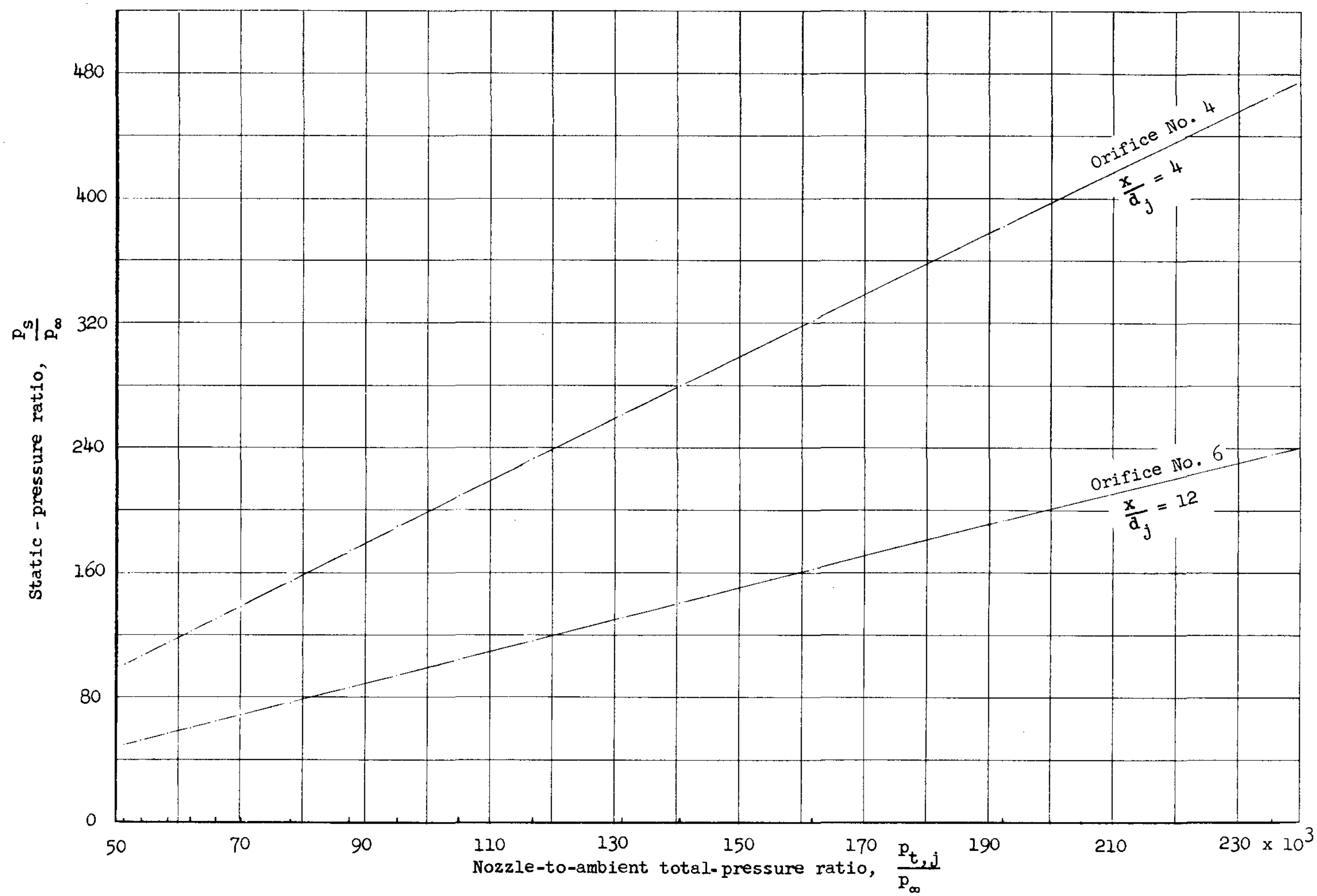

(a) $\frac{y}{d_j} = 7.$

Figure 6.- Typical variation of surface static pressure ratio with nozzle-to-ambient total-pressure ratios for constant distances downstream from nozzle exit. $M_j = 1.0$; $d_j = 0.125$ in.

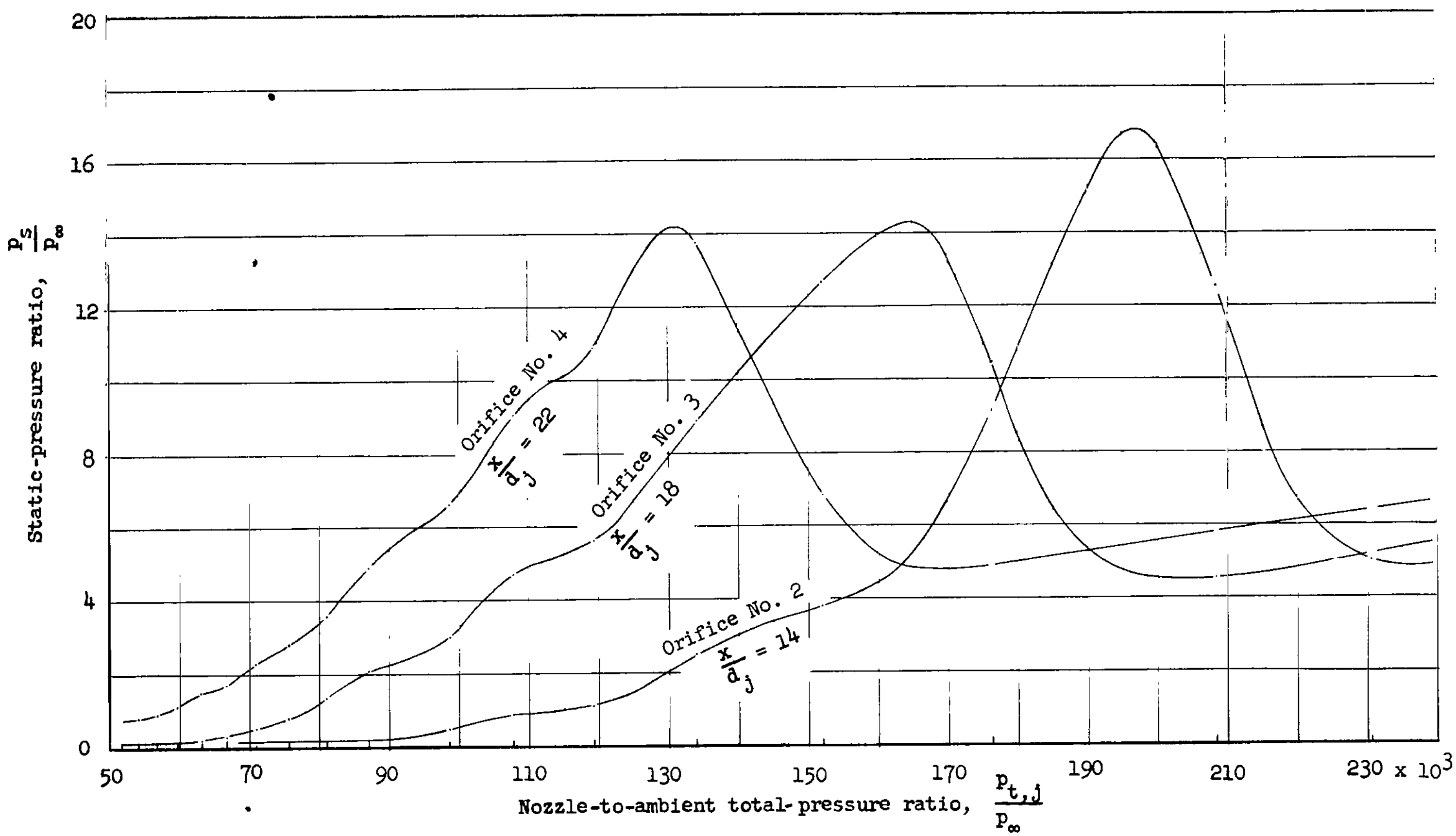

(b) $\frac{y}{d_j} = 60$.

Figure 6.- Concluded.

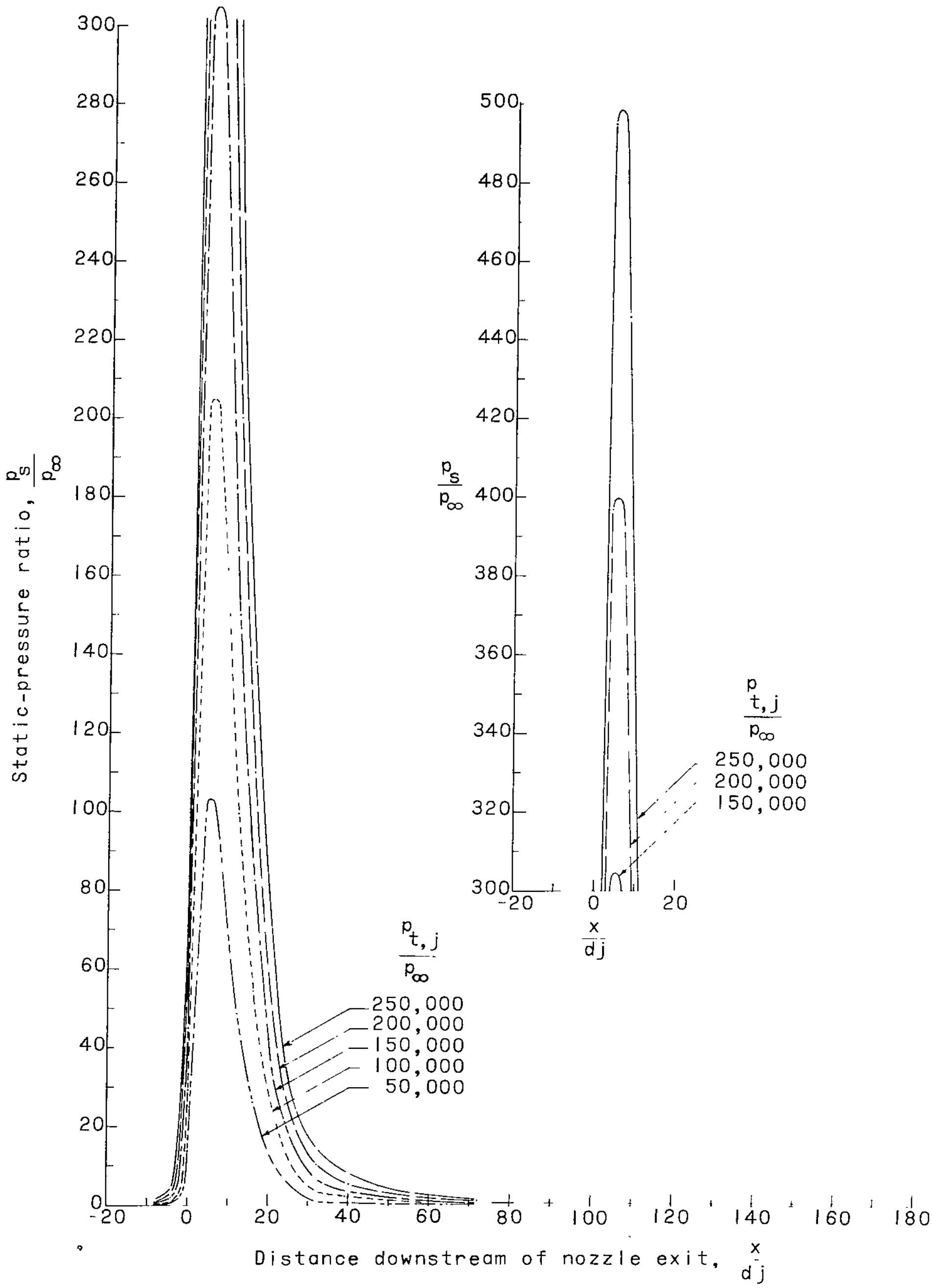

(a) $\frac{y}{d_j} = 7.$

Figure 7.- Distribution of impingement surface static-to-ambient pressure ratio for various nozzle total-to-ambient pressure ratios. $M_j = 1.0$; $d_j = 0.125$ in.; $\psi = 0^\circ$.

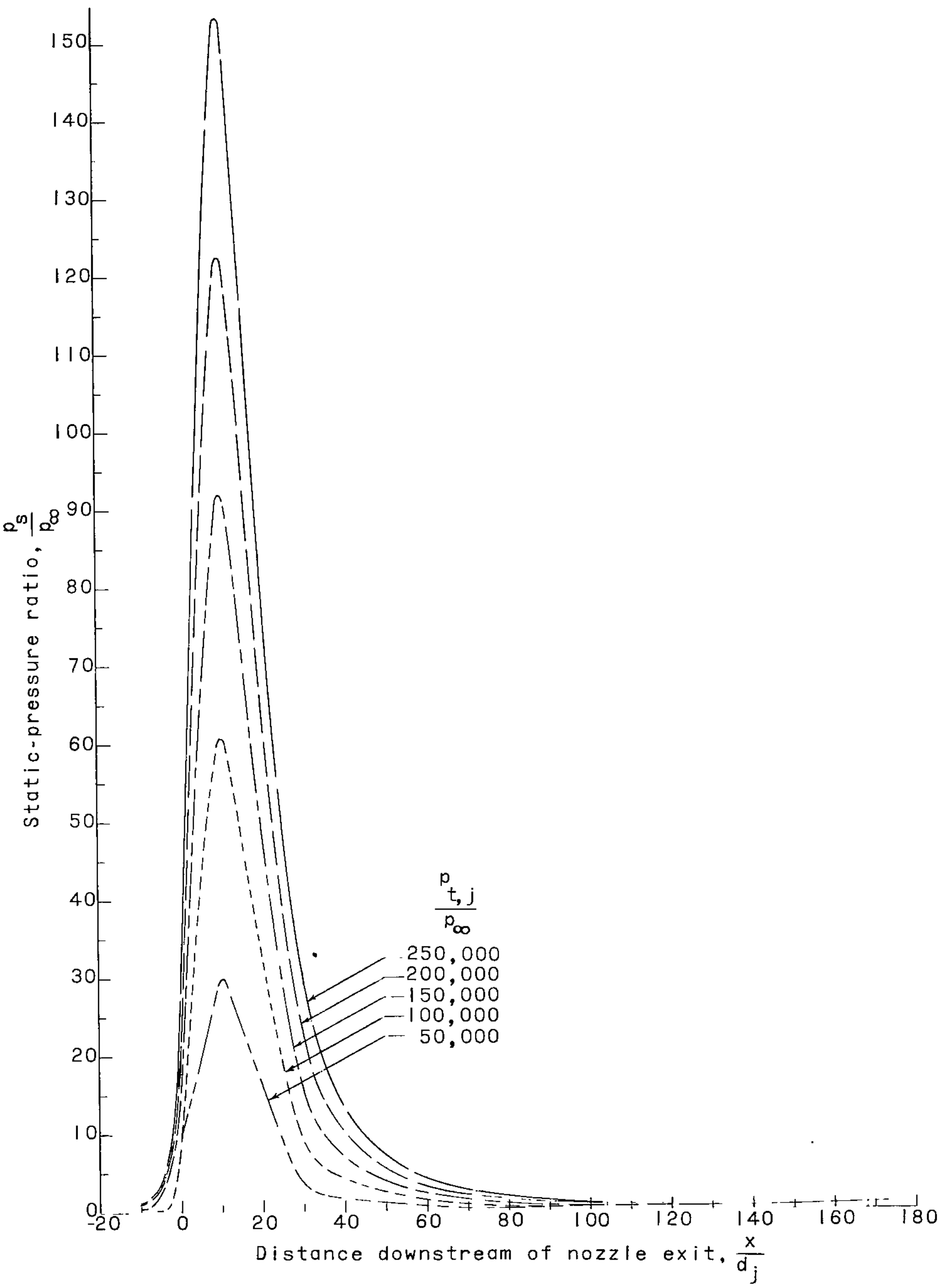

(b) $\frac{y}{d_j} = 14$.

Figure 7.- Continued.

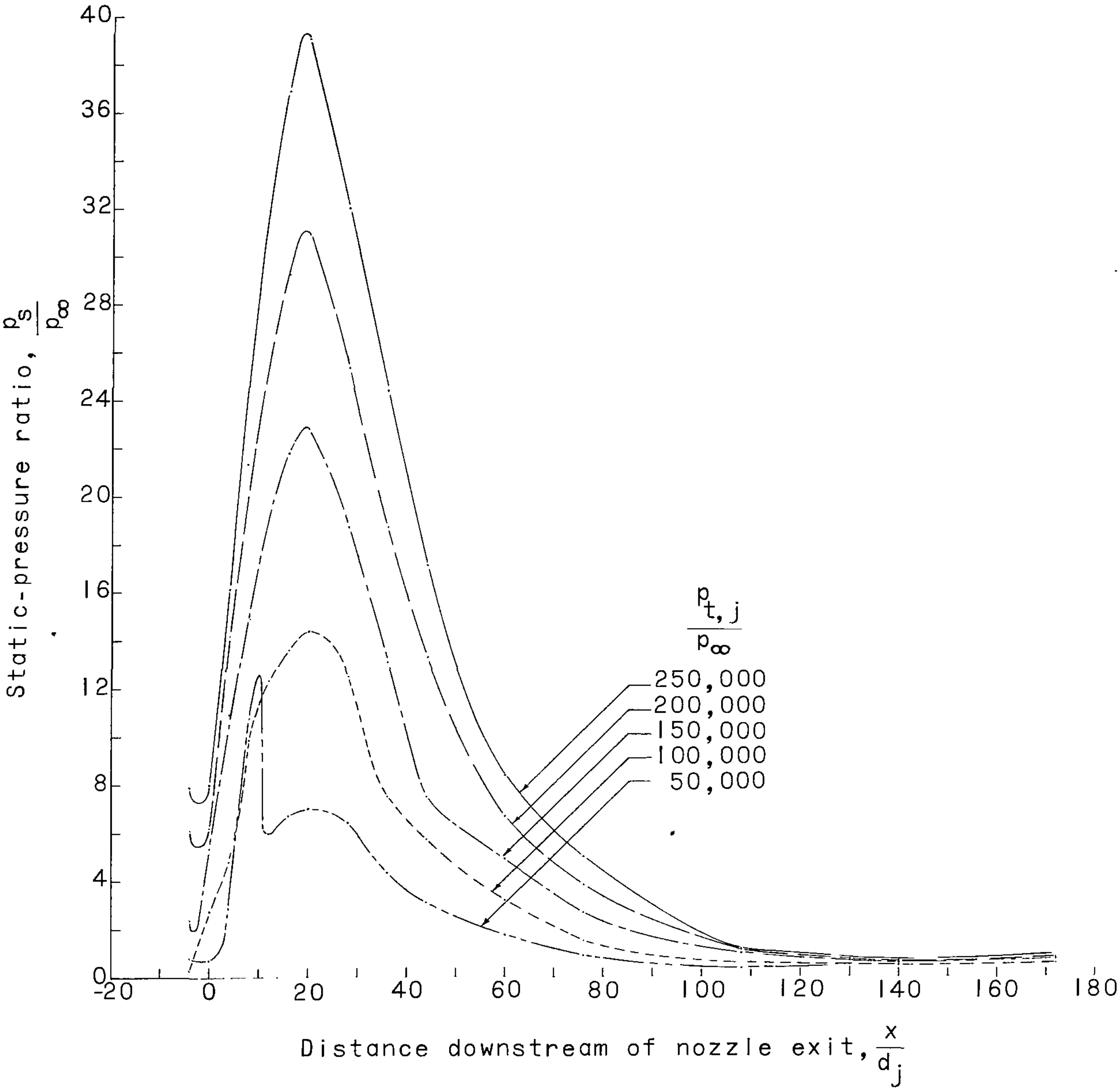

(c) $\frac{y}{d_j} = 30.$

Figure 7.- Continued.

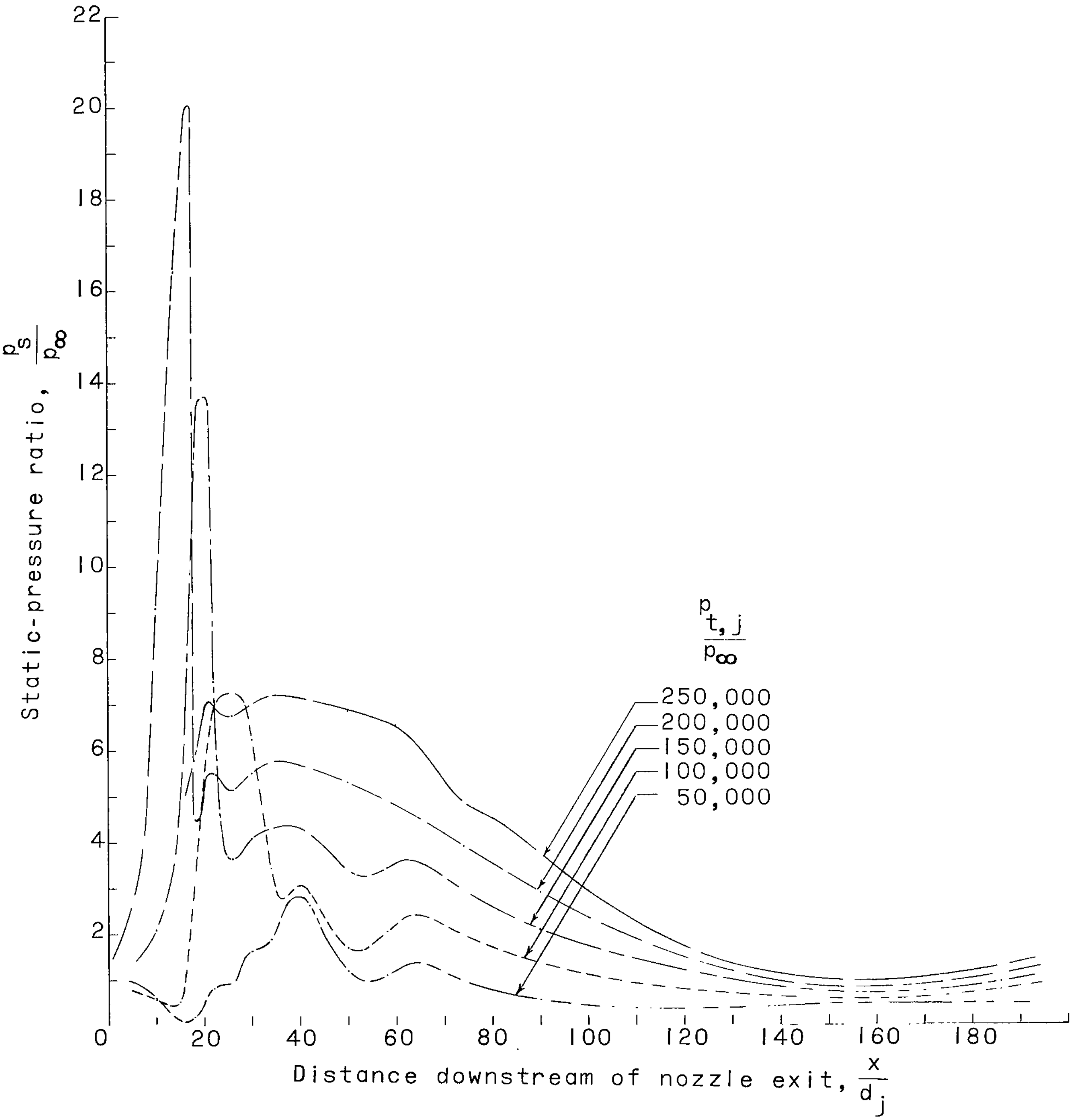

(d) $\frac{y}{d_j} = 60.$

Figure 7.- Concluded.

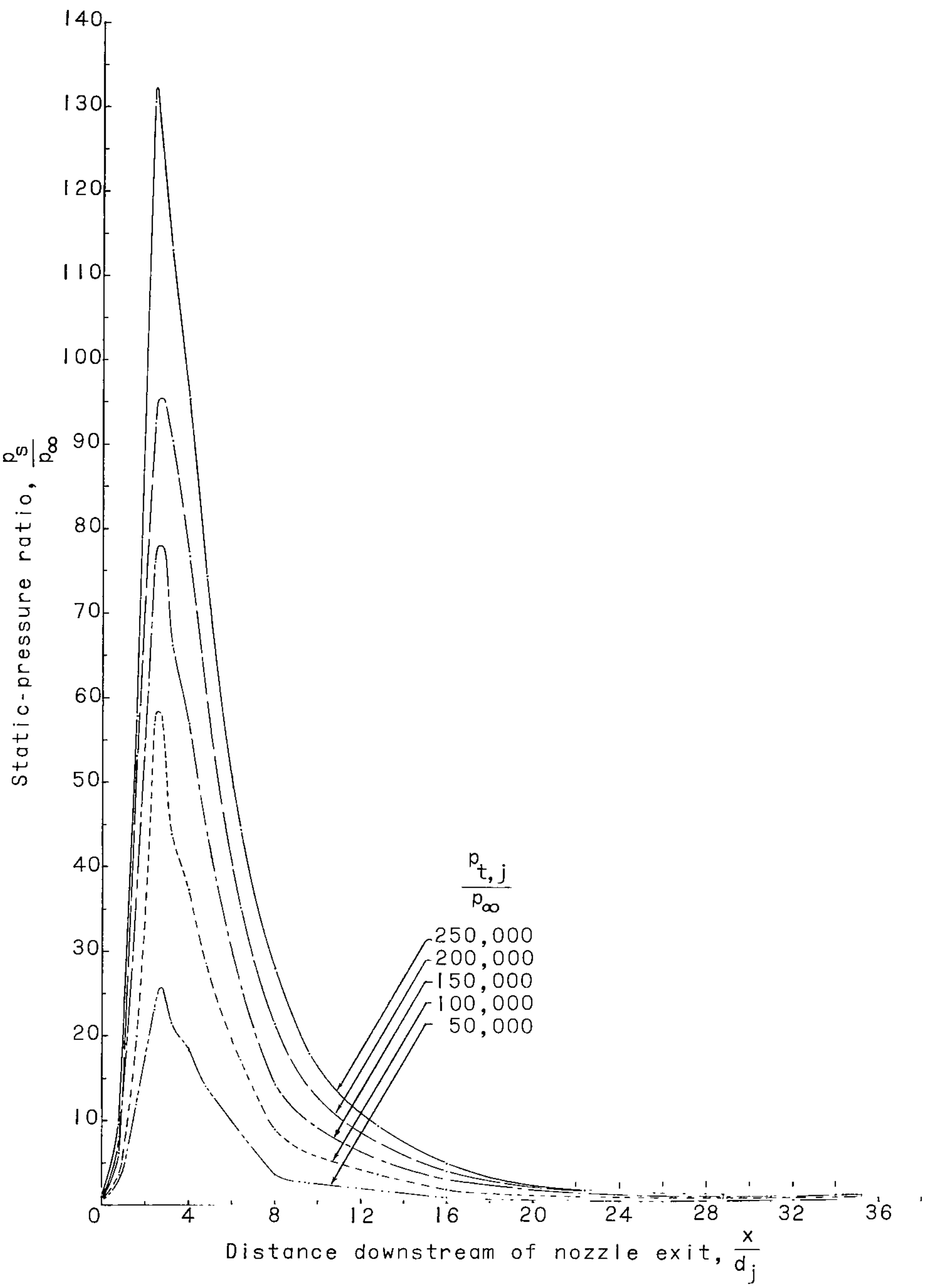

(a) $\frac{y}{d_j} = 2$.

Figure 8.- Distribution of impingement surface static-to-ambient pressure ratios for various nozzle total-to-ambient pressure ratios. $M_j = 5.0$; $d_j = 0.625$; $\psi = 0^{\circ}$.

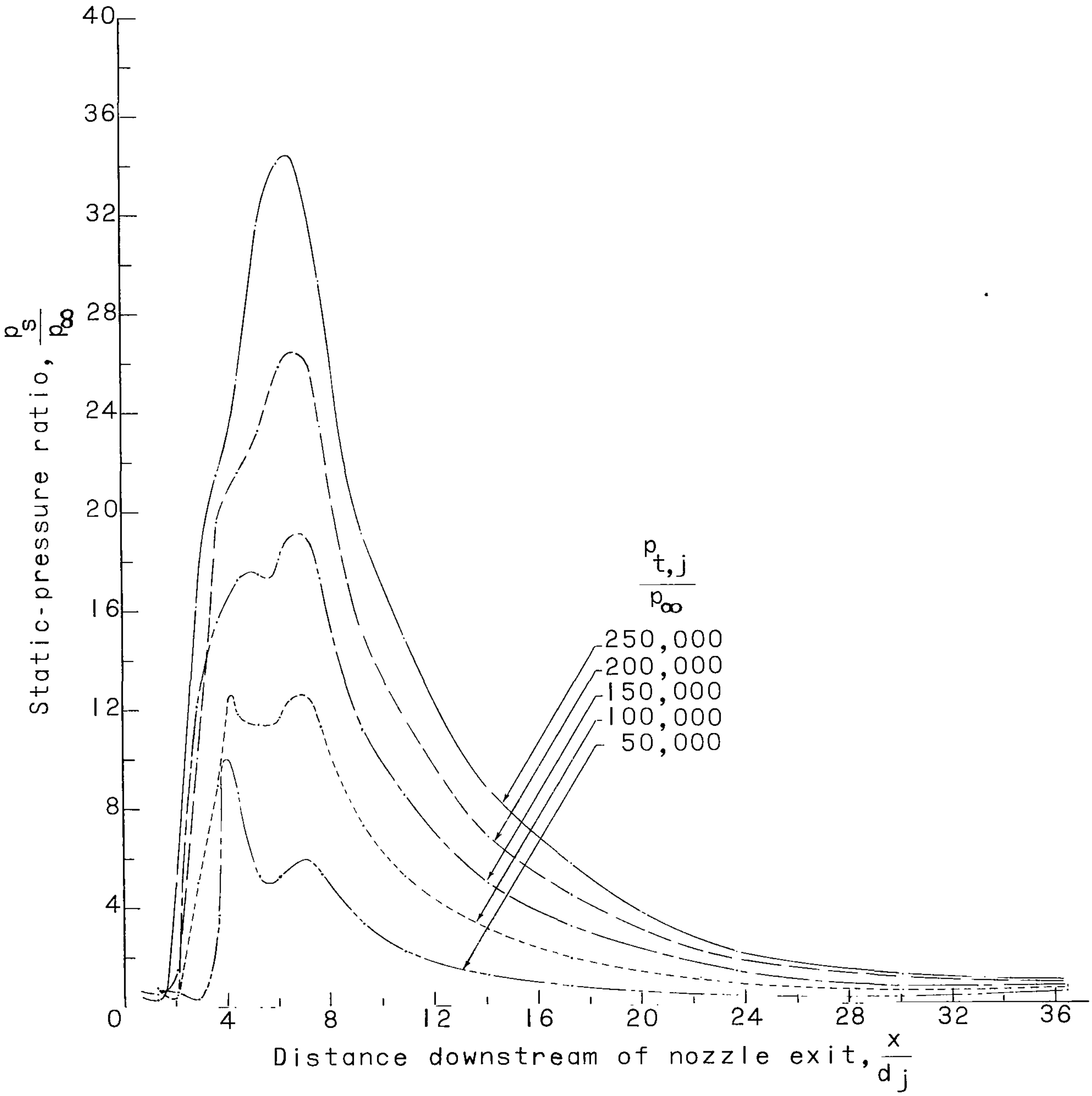

(b) $\frac{y}{d_j} = 4$.

Figure 8.- Continued.

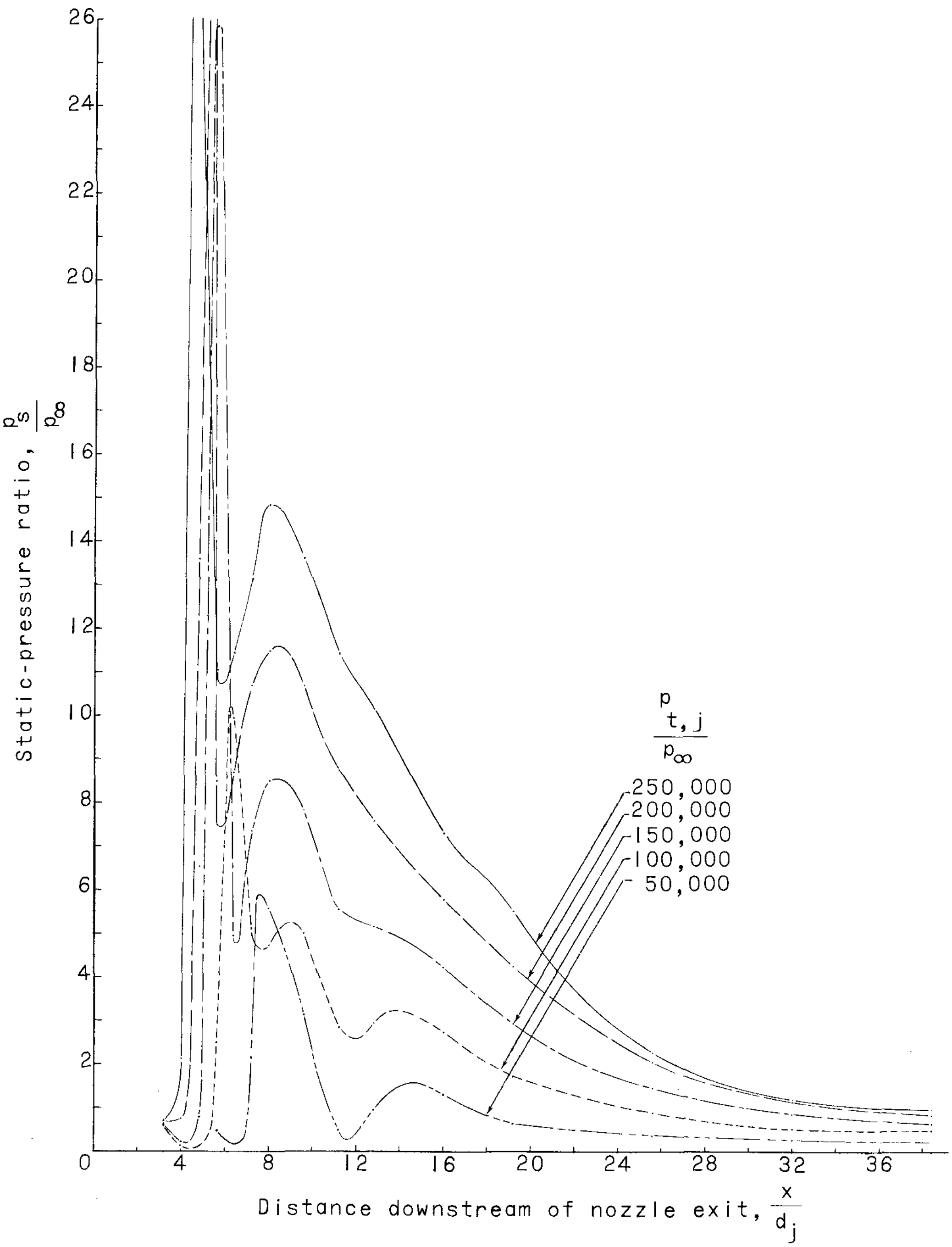

(c) $\frac{y}{d_j} = 6.$

Figure 8.- Continued.

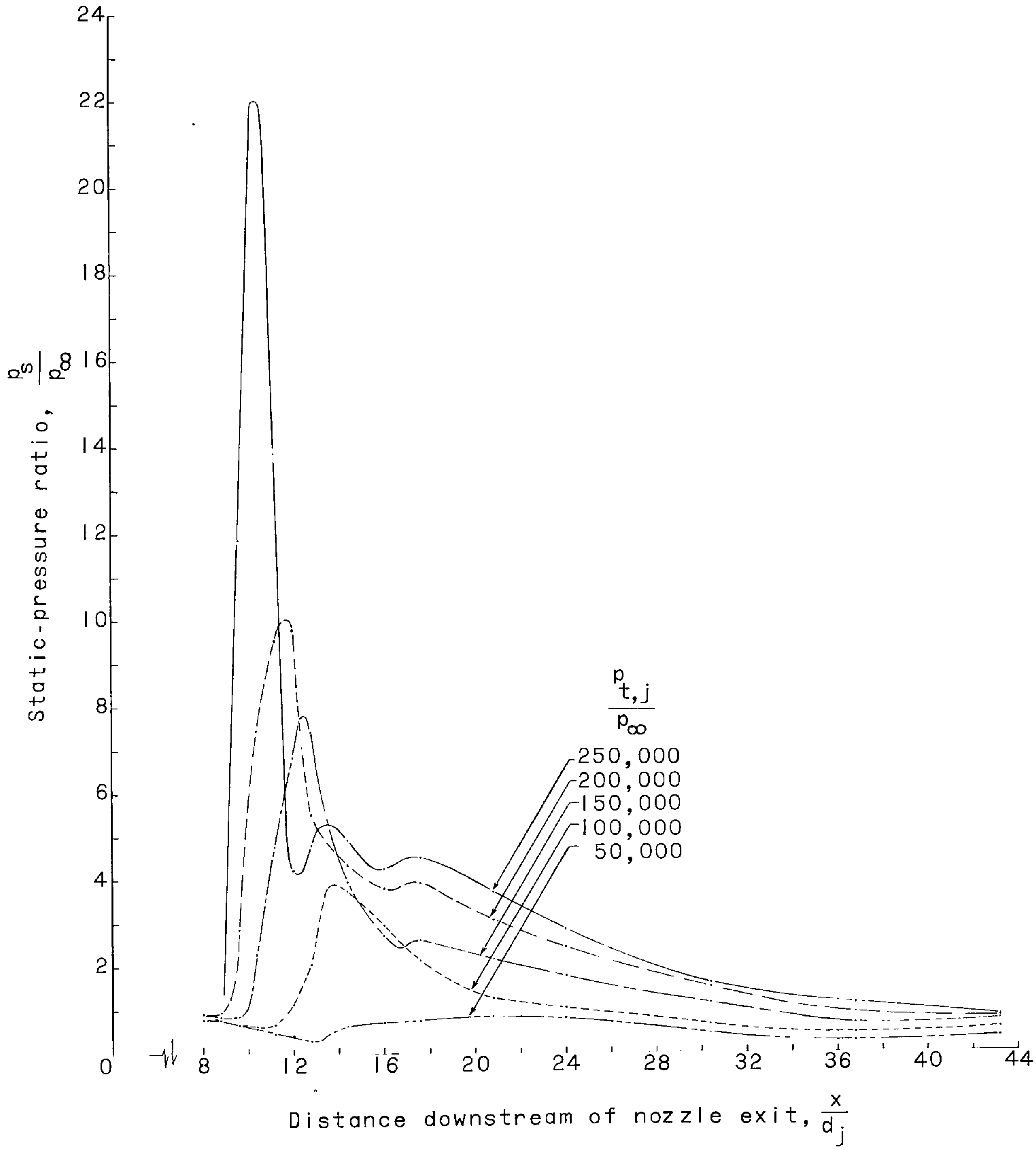

(d) $\frac{y}{d_j} = 10.$

Figure 8.- Concluded.

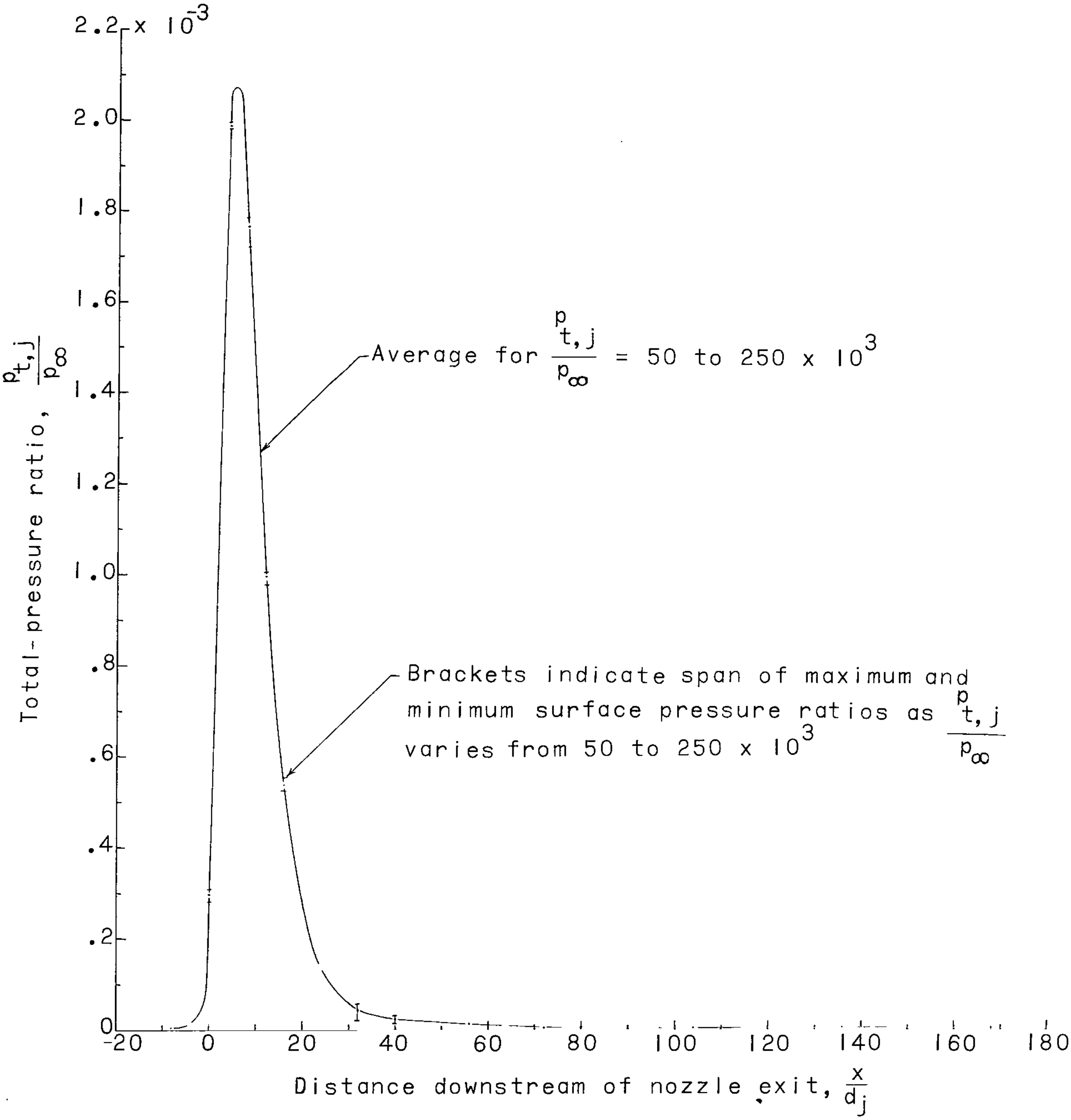

(a) $\frac{y}{d_j} = 7.$

Figure 9.- Distribution of impingement surface static-to-nozzle total pressure ratio for various nozzle total-to-ambient pressure ratios. $M_j = 1.0$; $d_j = 0.125$ in.; $\psi = 0^o$.

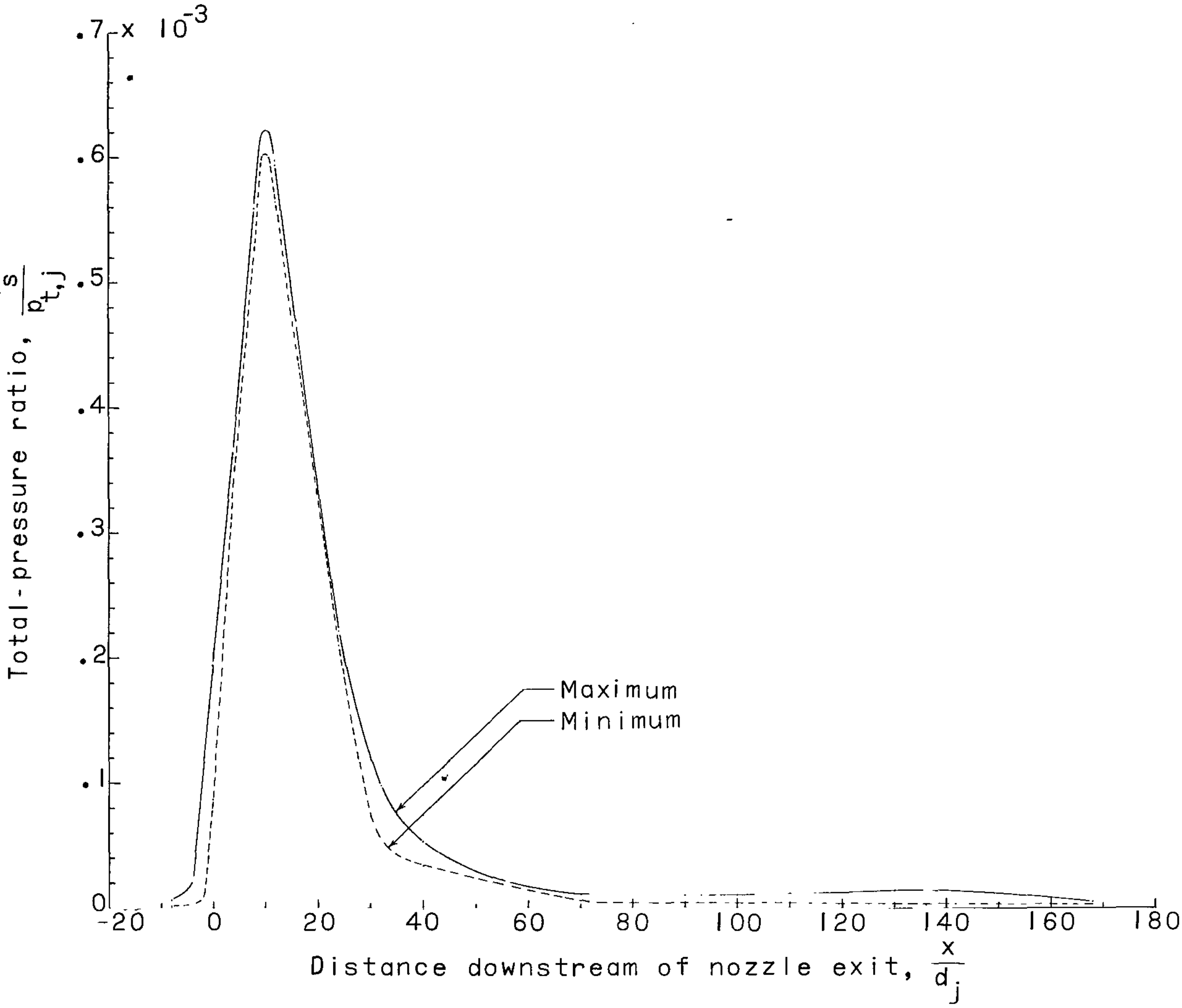

(b) $\frac{y}{d_j} = 14$.

Figure 9.- Continued.

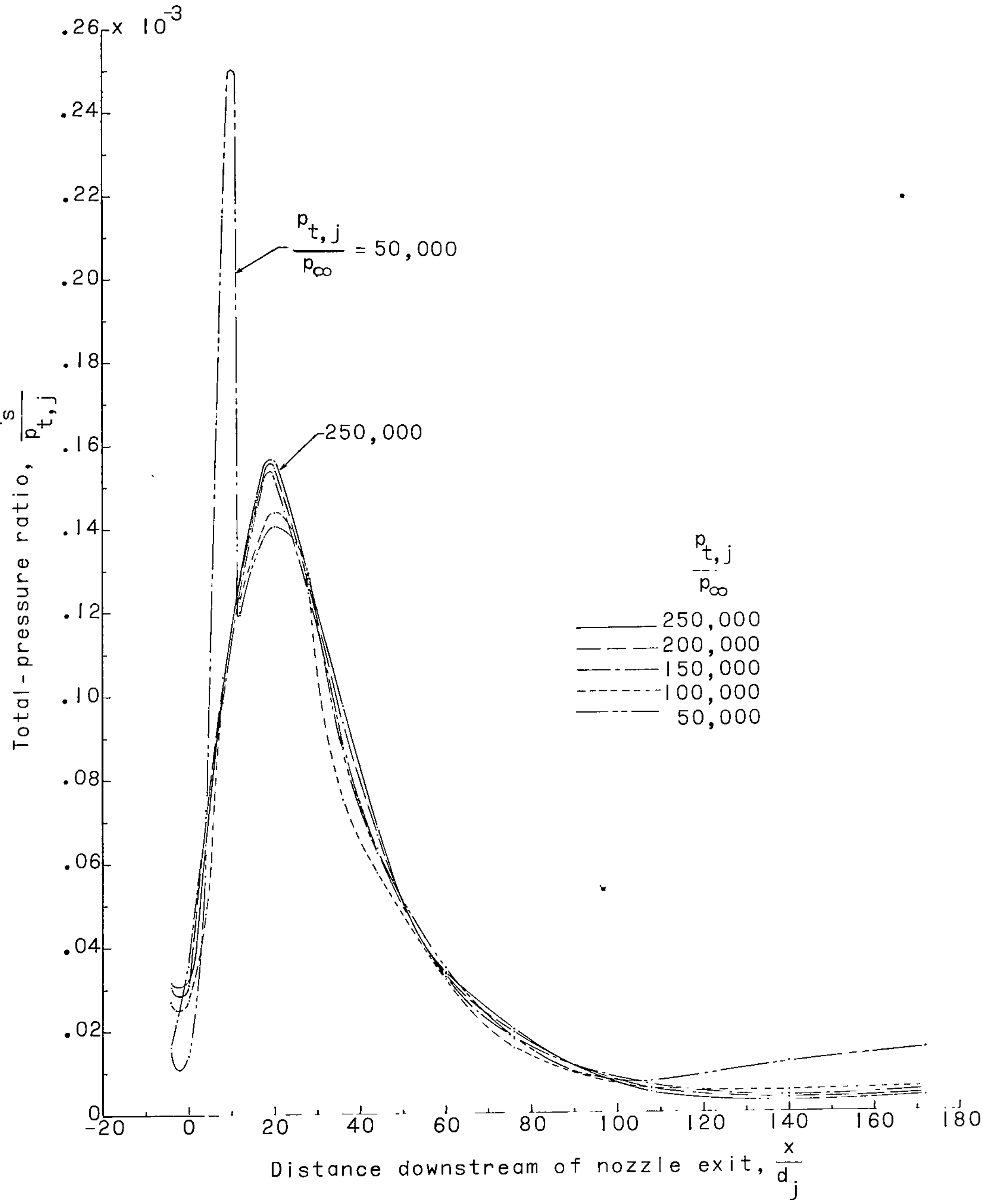

(c) $\frac{y}{d_j} = 30.$

Figure 9.- Continued.

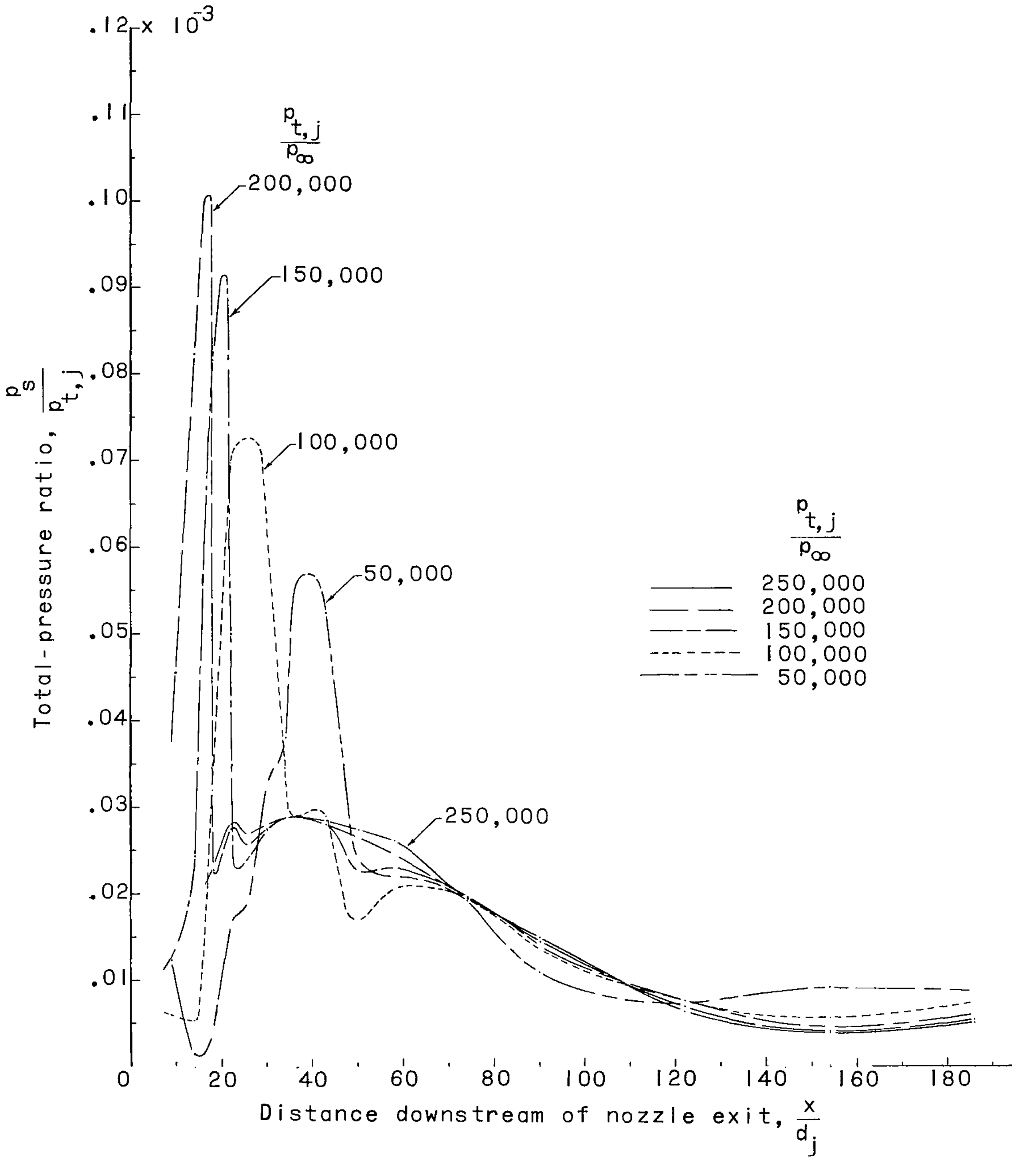

(d) $\frac{y}{d_j} = 60.$

Figure 9.- Concluded.

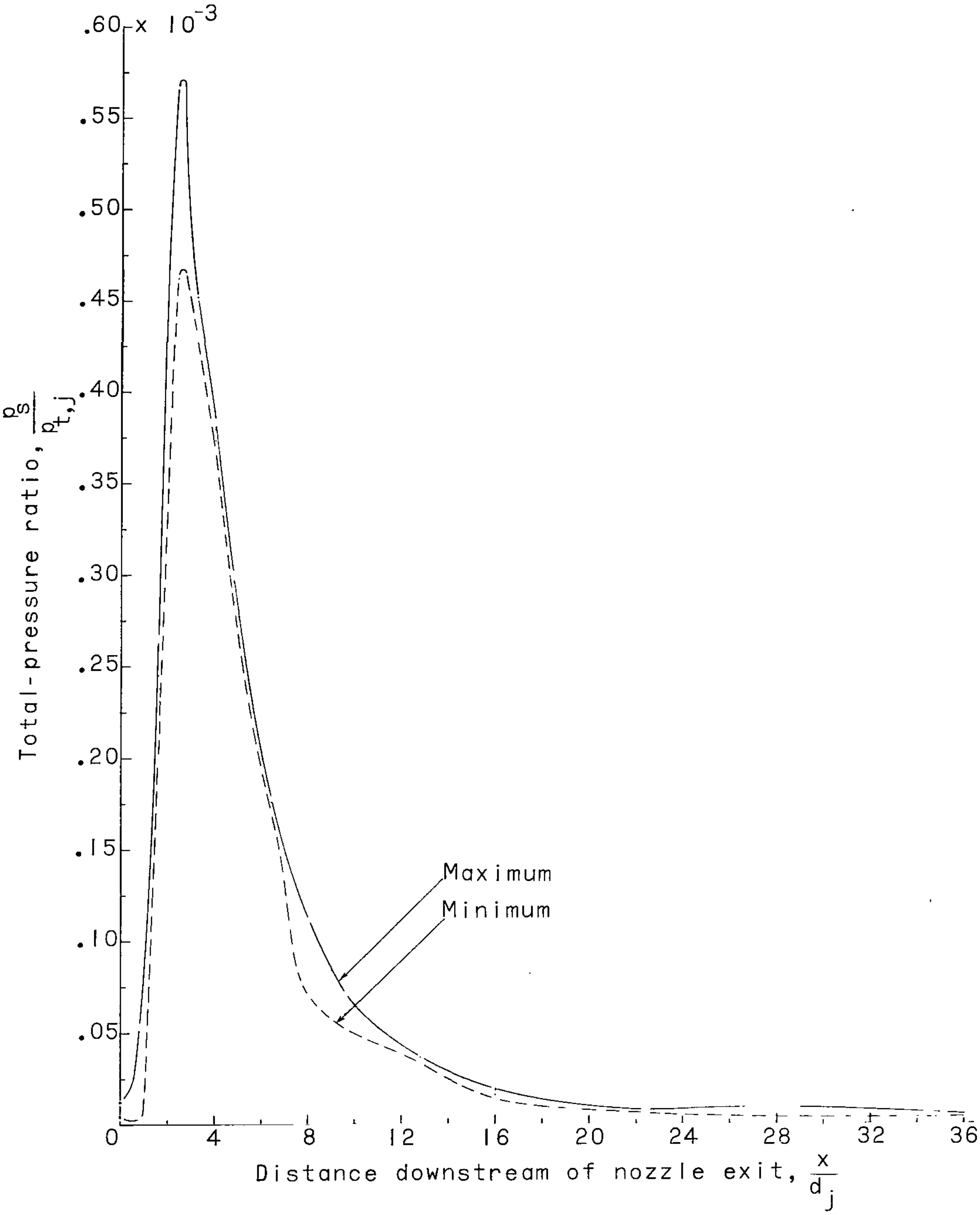

(a) $\frac{y}{d_j} = 2.$

Figure 10.- Distribution of impingement surface static-to-nozzle total-pressure ratio for various nozzle total-to-ambient pressure ratios. $M_j = 5.0$; $d_j = 0.625$ in.; $\psi = 0^{\circ}$.

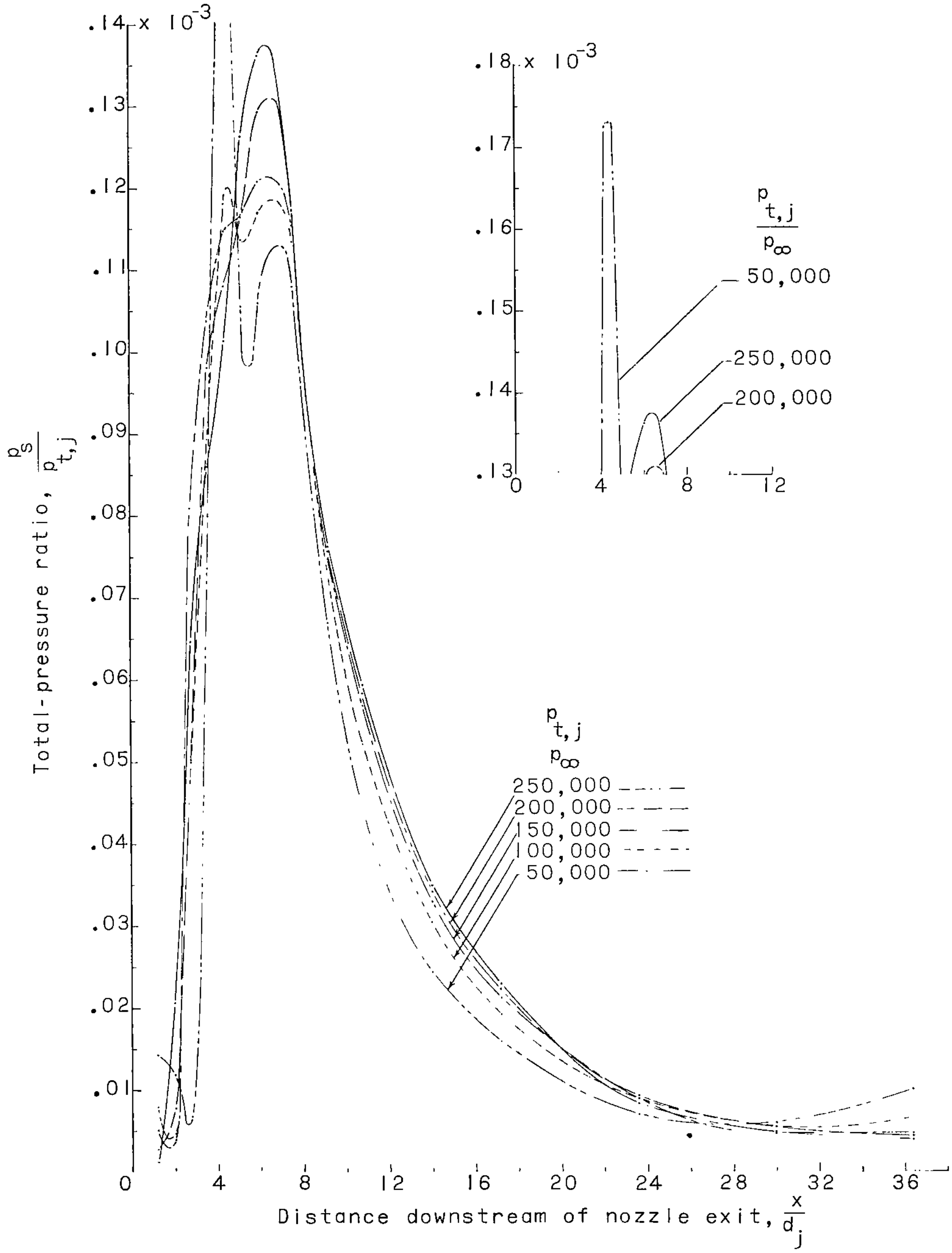

(b) $\frac{y}{d_j} = 4.$

Figure 10.- Continued.

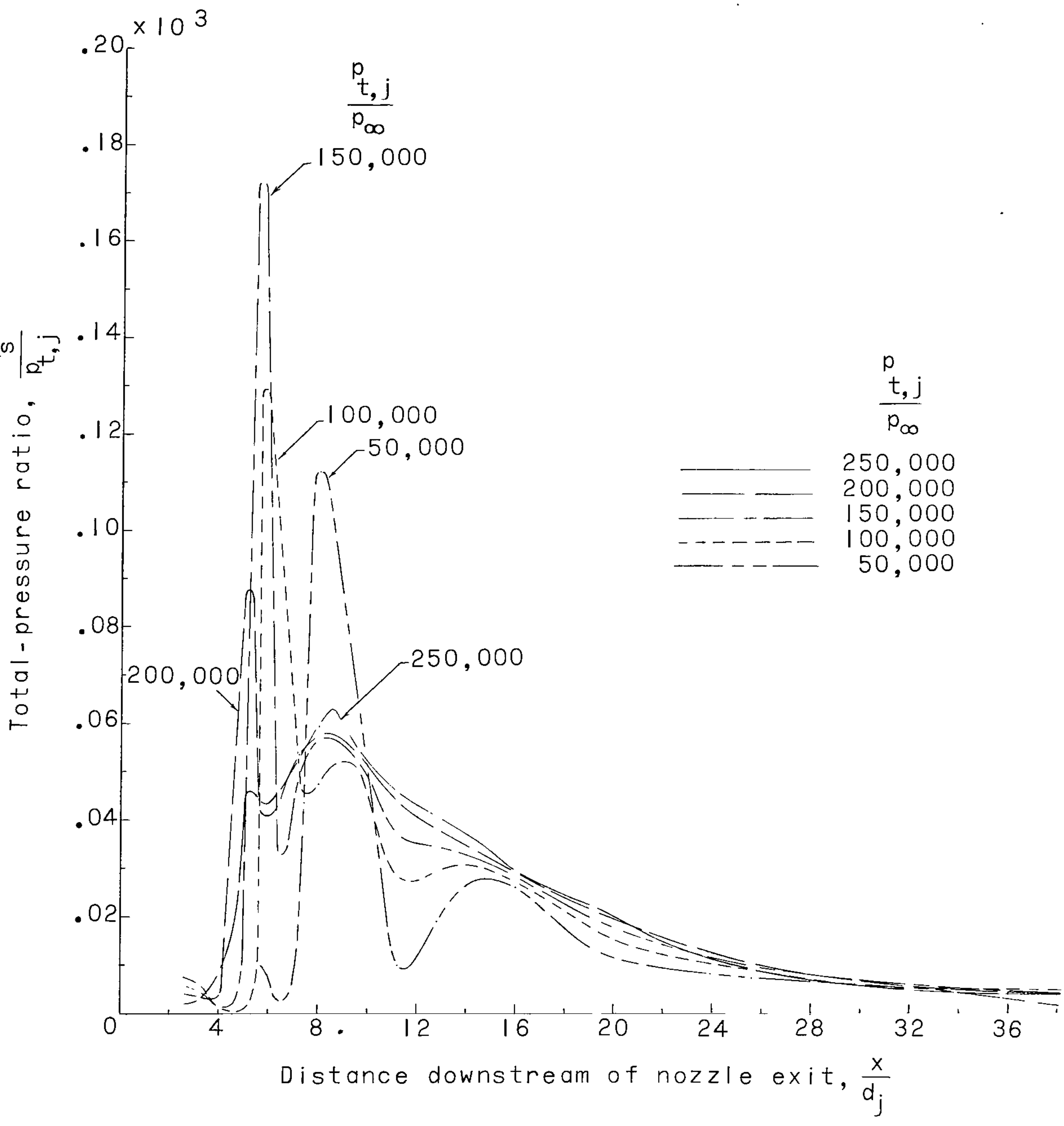

(c) $\frac{y}{d_j} = 6.$

Figure 10.- Continued.

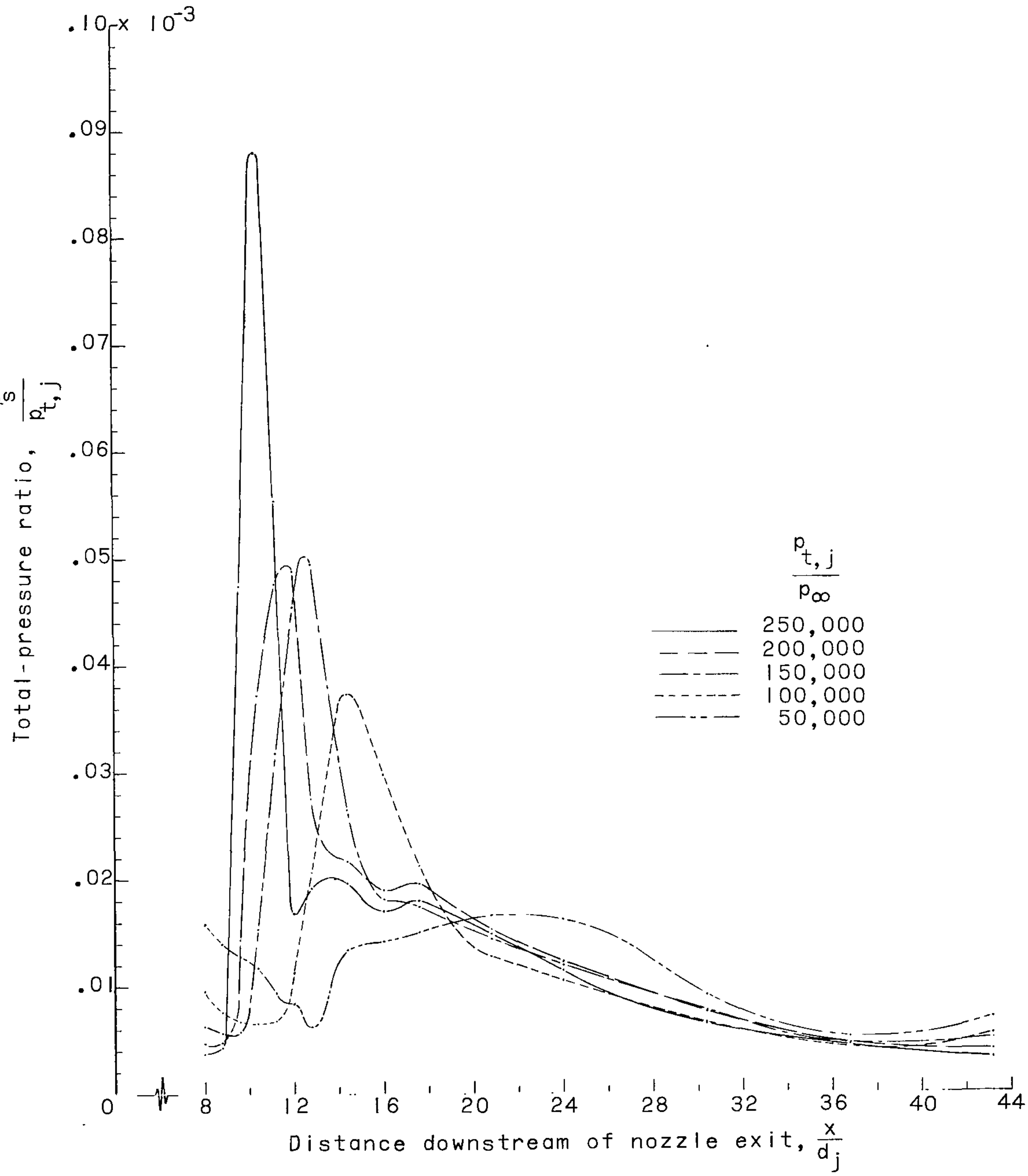

(d) $\frac{y}{d_j} = 10.$

Figure 10.- Concluded.

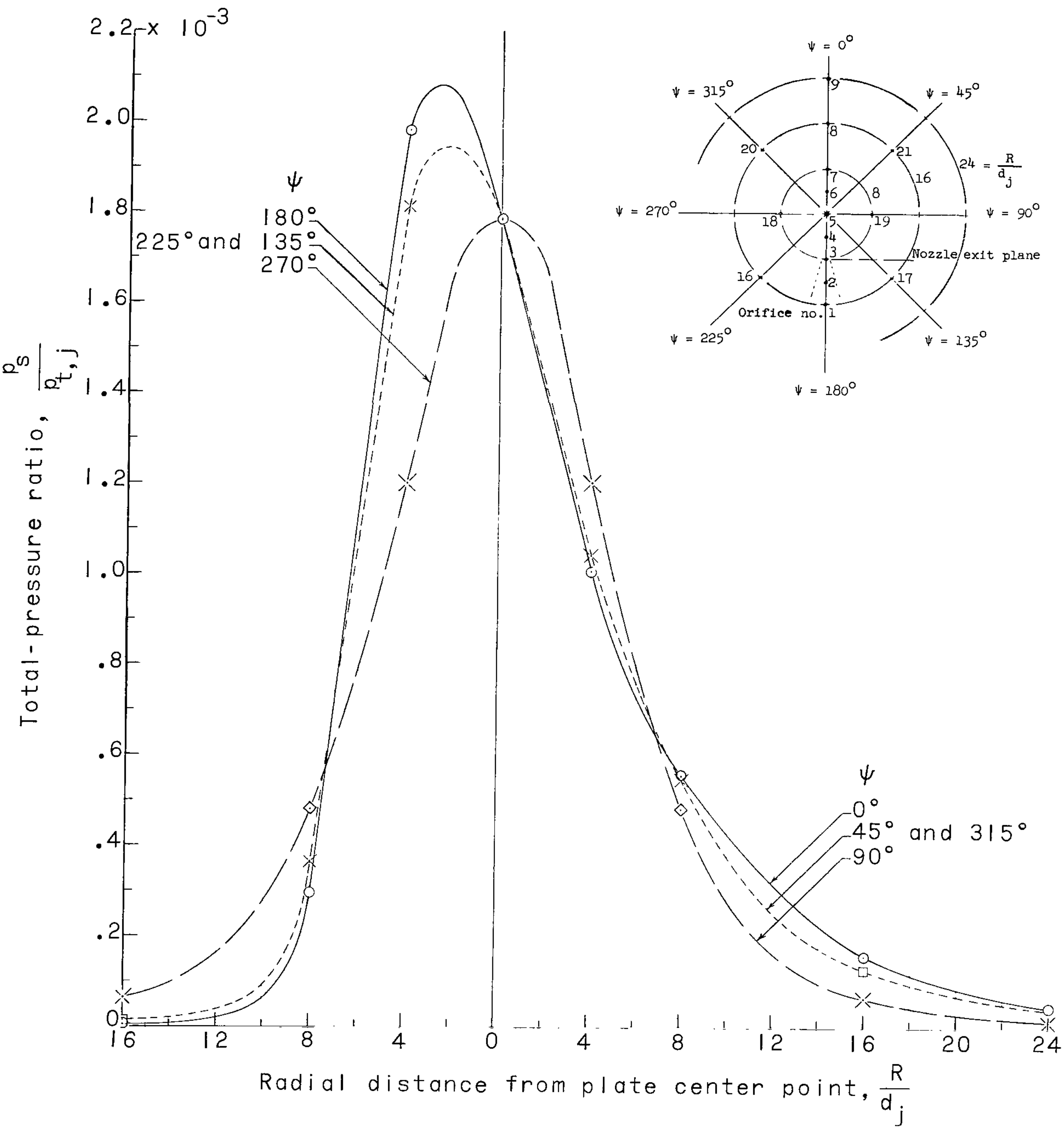

(a) Radial distribution.

Figure 11.- Radial and circumferential distributions of impingement surface static-to-nozzle total-pressure ratio. $M_j = 1.0$; $d_j = 0.125$ in., $\frac{y}{d_j} = 7$; $\frac{p_{t,j}}{p_\infty} = 250{,}000$.

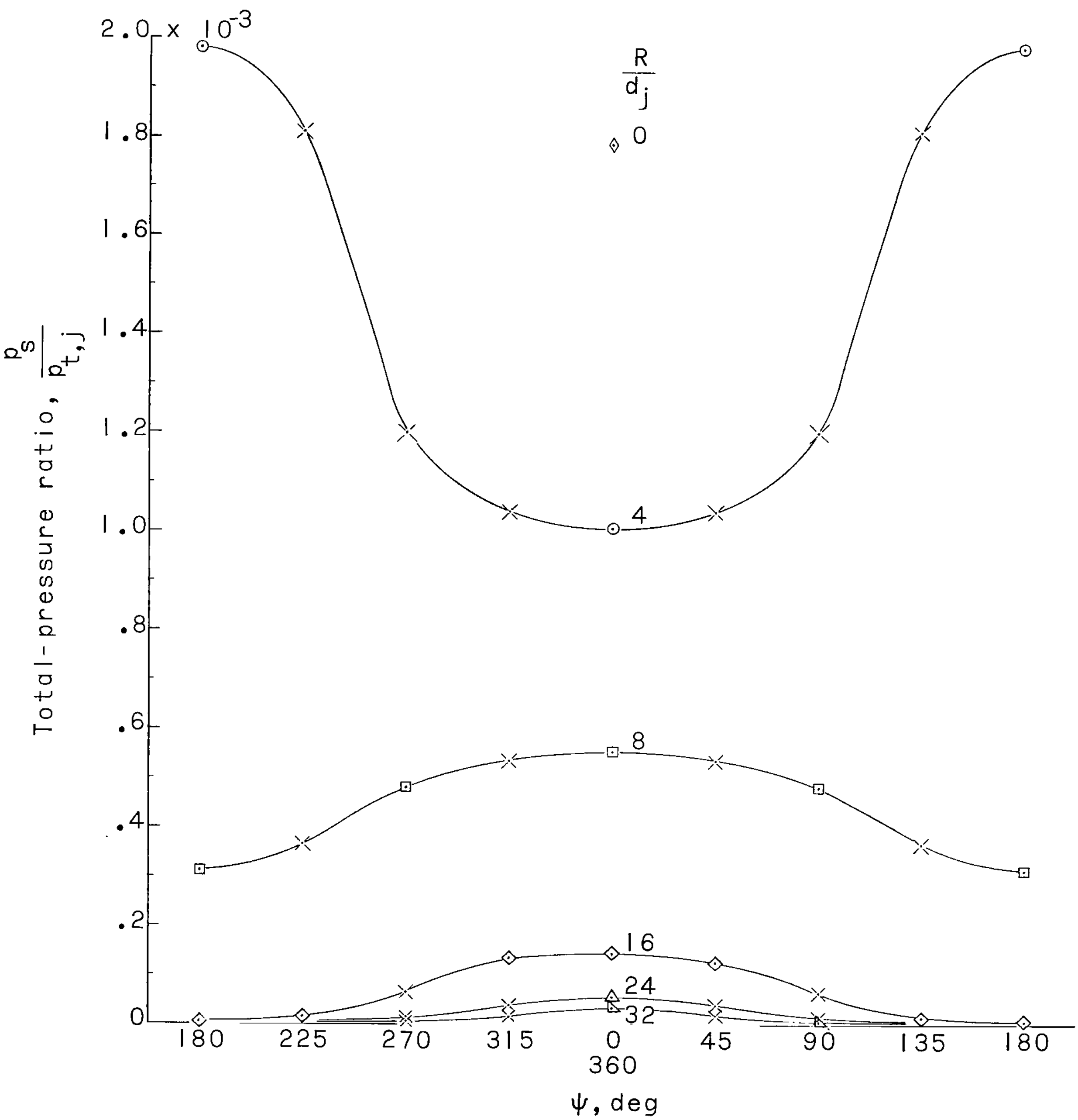

(b) Circumferential distribution.

Figure 11.- Concluded.

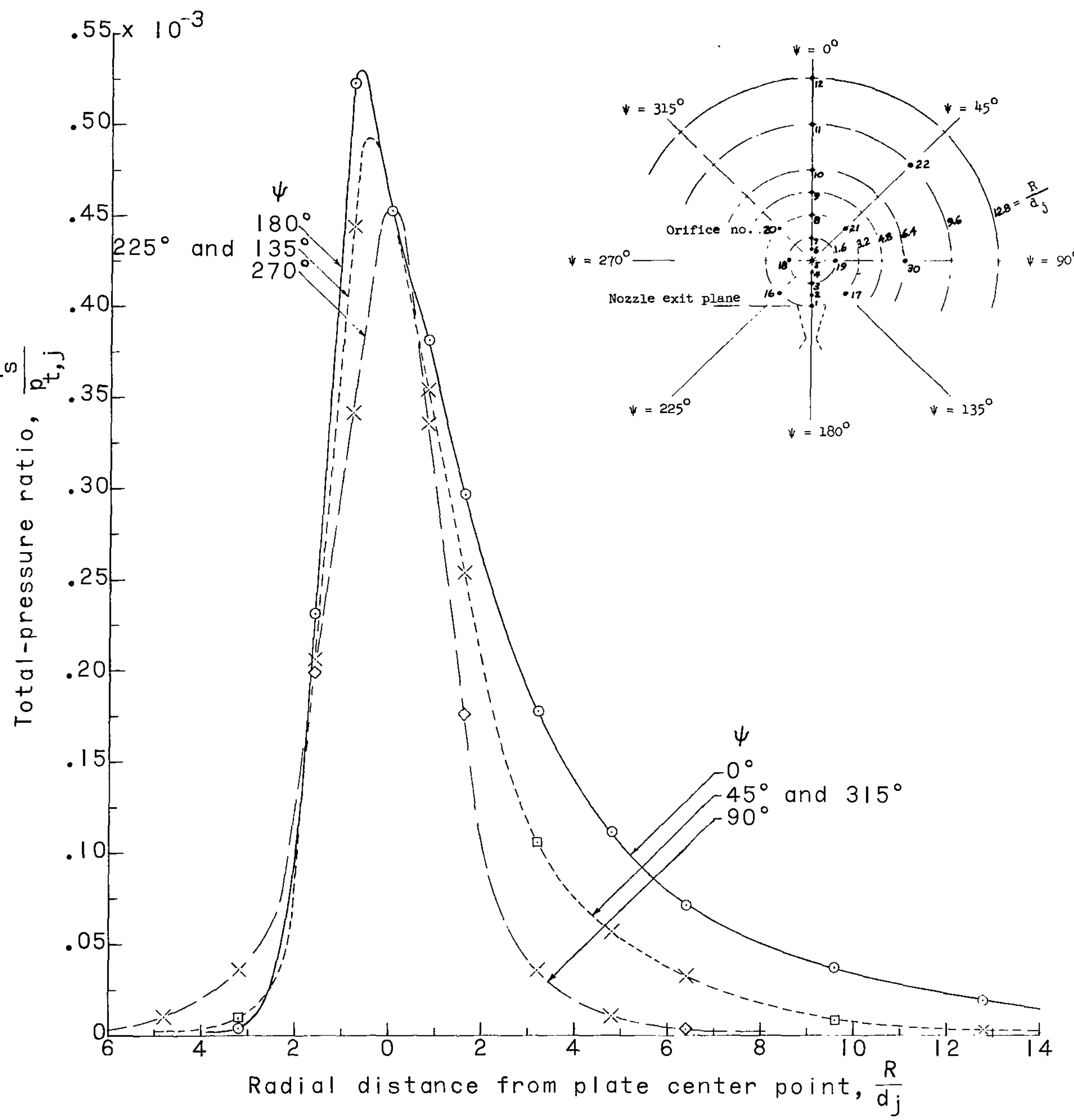

(a) Radial distribution.

Figure 12.- Radial and circumferential distributions of impingement surface static-to-nozzle total-pressure ratio. $M_j = 5.0$; $d_j = 0.625$ in.; $\frac{y}{d_j} = 2$; $\frac{p_{t,j}}{p_\infty} = 250{,}000$.

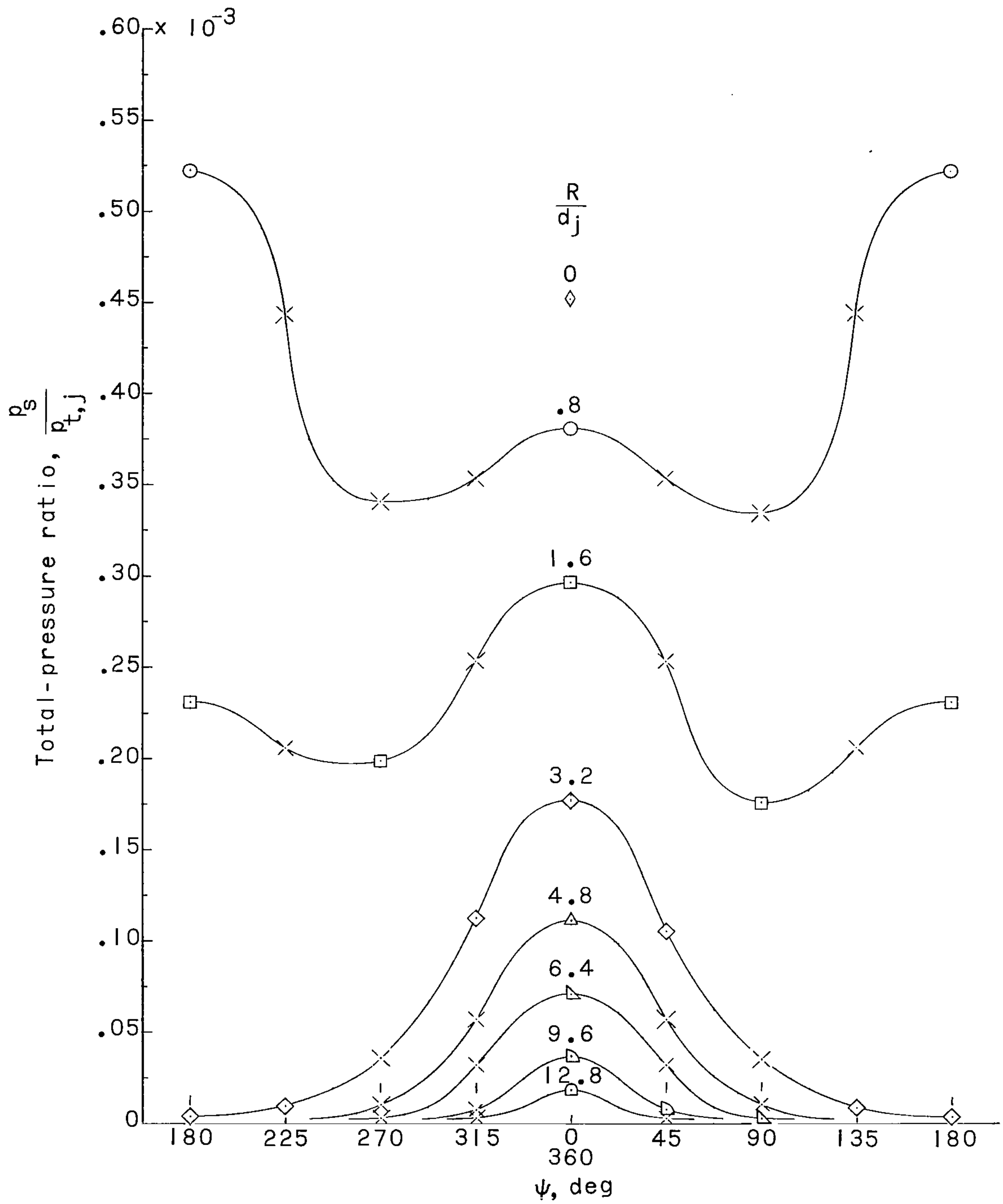

(b) Circumferential distribution.

Figure 12.- Concluded.

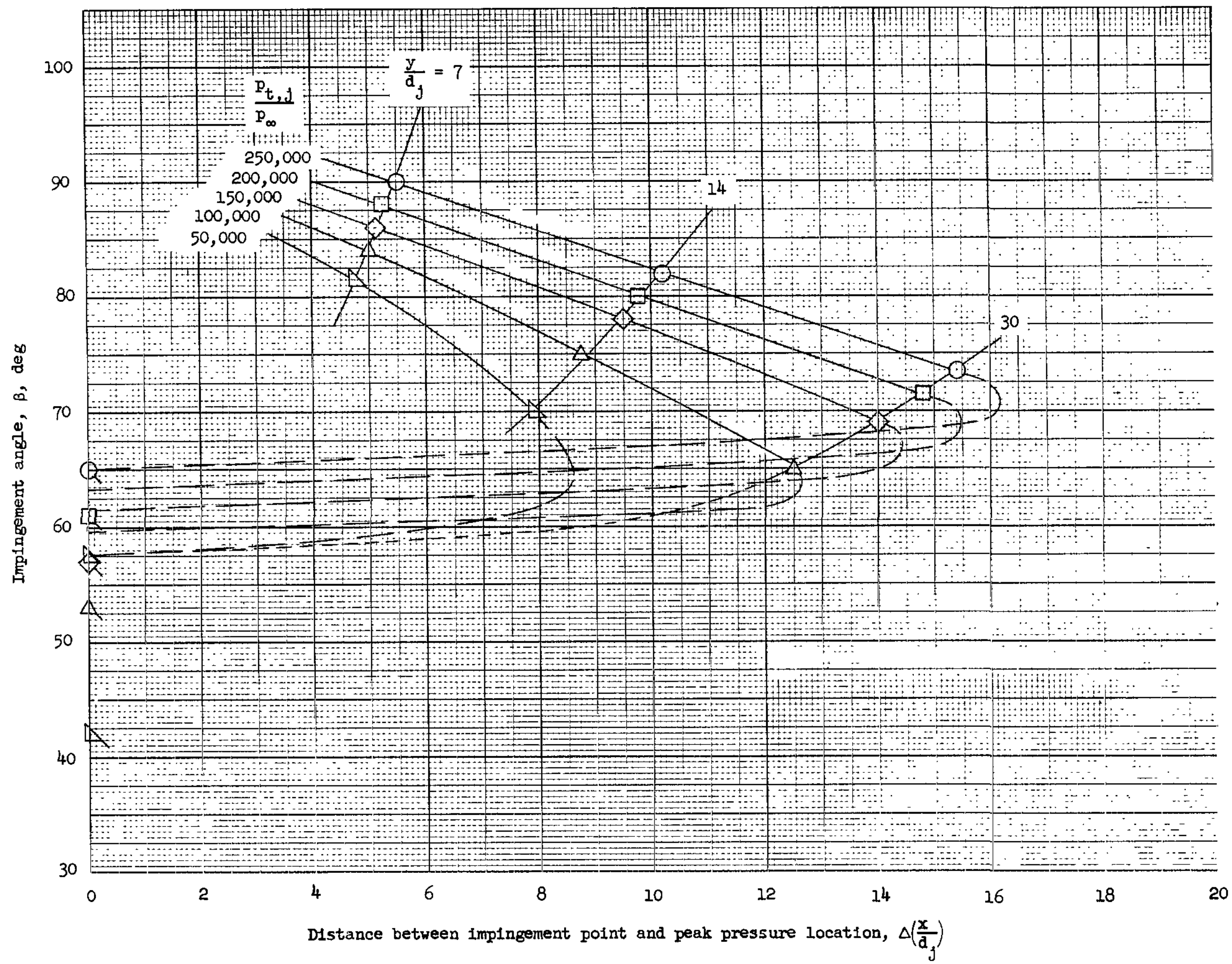

(a) $M_j = 1.0$. Flagged symbols are for $\frac{y}{d_j} = 60$.

Figure 13.- Variation of impingement angle with distance between impingement point and peak pressure location $\psi = 0^{\circ}$. Dashed lines indicate extrapolation.

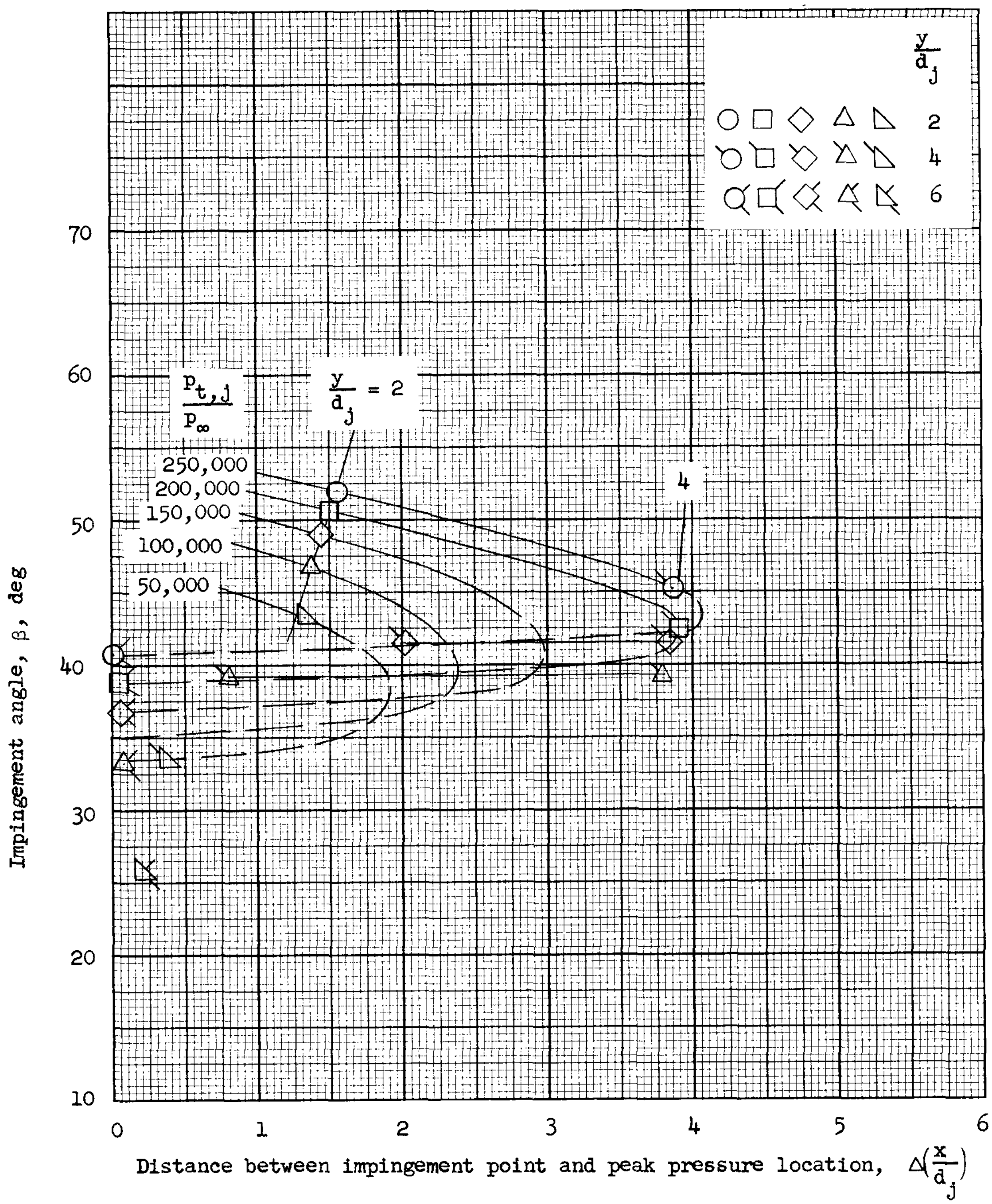

(b) $M_j = 5.0$. Note that for some pressure ratios there are two pressure peaks on same curve for $\frac{y}{d_j} = 4$.

Figure 13.- Concluded.

2171 ds

"The aeronautical and space activities of the United States shall be conducted so as to contribute . . . to the expansion of human knowledge of phenomena in the atmosphere and space. The Administration shall provide for the widest practicable and appropriate dissemination of information concerning its activities and the results thereof."

—NATIONAL AERONAUTICS AND SPACE ACT OF 1958

NASA SCIENTIFIC AND TECHNICAL PUBLICATIONS

TECHNICAL REPORTS: Scientific and technical information considered important, complete, and a lasting contribution to existing knowledge.

TECHNICAL NOTES: Information less broad in scope but nevertheless of importance as a contribution to existing knowledge.

TECHNICAL MEMORANDUMS: Information receiving limited distribution because of preliminary data, security classification, or other reasons.

CONTRACTOR REPORTS: Technical information generated in connection with a NASA contract or grant and released under NASA auspices.

TECHNICAL TRANSLATIONS: Information published in a foreign language considered to merit NASA distribution in English.

TECHNICAL REPRINTS: Information derived from NASA activities and initially published in the form of journal articles.

SPECIAL PUBLICATIONS: Information derived from or of value to NASA activities but not necessarily reporting the results of individual NASA-programmed scientific efforts. Publications include conference proceedings, monographs, data compilations, handbooks, sourcebooks, and special bibliographies.

Details on the availability of these publications may be obtained from:

SCIENTIFIC AND TECHNICAL INFORMATION DIVISION

NATIONAL AERONAUTICS AND SPACE ADMINISTRATION

Washington, D.C. 20546